(Rorsman and Trube, 1985). Under zero intracellular ATP, however, the input conductance only increased to 0.9 nS, >90% of which was attributed to $K_{ATP}$ conductance. This value was much smaller than the experimental measurements. However, we failed to improve $G_{KATP}$ of the original model of $I_{KATP}$ (Magnus and Keizer, 1998), and this problem was left for future work.

*$Ca^{2+}$-activated $K^+$ current ($I_{KCa(SK)}$).* In islet preparations, Göpel et al. (1999a) recorded a novel $K^+$ current component ($I_{Kslow}$), which was activated with a slow time constant of ~2.3 s during a train of depolarizing pulses and deactivated with a time constant of 6.5 s after the pulses. An analogous current was also recorded in dispersed mouse β cells in several studies (Göpel et al., 1999a; Goforth et al., 2002; Zhang et al., 2005; Düfer et al., 2009). The pharmacological and gene knockout studies have suggested that small-conductance $K_{Ca}$ (SK) channels might contribute substantially to $I_{Kslow}$ (Zhang et al., 2005; Düfer et al., 2009). Supporting this view, isoforms of SK −1 to −4 were found to be expressed at the level of mRNA and protein in mouse β cells (Tamarina et al., 2003; Düfer et al., 2009). Interestingly, Kanno et al. (2002) ascribed ~50% of the experimental $I_{Kslow}$ to $I_{KATP}$. Thus, we implemented the SK channel current as $I_{KCa(SK)}$ in our new model separately from $I_{KATP}$. The $Ca^{2+}$ dependency for activation of $I_{KCa(SK)}$ was adopted from Hirschberg et al. (1998) (Eq. S38). It seems that the activation by $Ca^{2+}$ of SK current is almost instantaneous, but slow changes in $[Ca^{2+}]_i$ and/or the contaminated $I_{KATP}$ component might result in the slow time course of $I_{Kslow}$ in experimental recordings.

*Background nonselective cation current ($I_{bNSC}$).* Henquin and Meissner (1984a) showed that the resting membrane potential of β cells is less negative than the $K^+$ equilibrium potential. They attributed this depolarizing effect to a basal membrane $Na^+$ conductance (see also Ashcroft and Rorsman, 1989). It is now well established that this background $Na^+$ conductance includes several types of currents. Nevertheless, a background cation current is still required to establish the resting potential, especially when $I_{CRAN}$ is largely inactivated. Thus, we added such a current, $I_{bNSC}$, of an unspecified nature. Note that many previous β-cell models also included a background current component (Chay and Keizer, 1983; Chay, 1996; Magnus and Keizer, 1998; Meyer-Hermann, 2007; Fridlyand et al., 2009). $I_{bNSC}$ in this model is permeable to $Na^+$ and $K^+$ with a reversal potential at approximately −20 mV (Eqs. S40–S42). The conductance was adjusted to give both the resting membrane potential and input impedance consistent with experimental measurements at a low [G] (Rorsman et al., 1986; Rorsman and Trube, 1986).

*Plasma membrane $Ca^{2+}$ pump (PMCA) and $Na^+/Ca^{2+}$ exchange (NCX) currents ($I_{PMCA}$, $I_{NaCa}$).* $Ca^{2+}$ influx through $I_{CaV}$ is balanced with $Ca^{2+}$ efflux via $I_{PMCA}$ (PMCA1, 2, and 3) and $I_{NaCa}$ (NCX1) (Váradi et al., 1995; Herchuelz et al., 2007). PMCA has one $Ca^{2+}$-binding site and 1:1 $Ca^{2+}$/ATP stoichiometry (Brini and Carafoli, 2009). PMCA2 has an apparent Hill coefficient of ~2 (Caride et al., 2001) and the half-maximal concentration of ~0.1 μM $[Ca^{2+}]_i$ in the presence of calmodulin (Enyedi et al., 1991; Elwess et al., 1997). Based on these findings, $I_{PMCA}$ is expressed by a Hill equation (Eq. S95). In addition, it is known that PMCA exchanges one intracellular $Ca^{2+}$ for one extracellular $H^+$ (Hao et al., 1994), and we assumed that the excess $H^+$ was instantaneously removed by $Na^+/H^+$ exchange. Because $Na^+/H^+$ exchange was not included in the present model, the resultant $Na^+$ influx by the functional coupling of PMCA and $Na^+/H^+$ exchange was directly included in calculating $d[Na^+]_i/dt$ (Eq. S3).

The description of $I_{NaCa}$ was adopted from a cardiac myocyte model (Takeuchi et al., 2006), which describes time-dependent transitions between different functional states of the NCX molecule (Eqs. S75–S94). The slope conductance of $I_{NaCa}$ near the reversal potential was 25.5 pS $pF^{-1}$ at 14 μM $[Ca^{2+}]_i$ and 30 mM $[Na^+]_i$ in the present model, which is about half of the experimental value (53 pS $pF^{-1}$) (Gall et al., 1999). This difference seems to fall within the range of experimental variations because of the limited intracellular perfusion with pipette solutions through the ruptured patch.

*NaK current ($I_{NaK}$).* The $I_{NaK}$ model was adopted from Oka et al. (2010), in which the turnover rate was precisely described in terms of $V_m$, intracellular, and extracellular compositions of $Na^+$ and $K^+$, and the free energy of ATP hydrolysis ($\Delta G_{ATP}$) based on thermodynamics (Eqs. S54–S74). Although this model was developed with reference to experimental measurements in cardiac myocytes, we assumed for convenience that the basic characteristics of the pump activity would be common in β cells. In addition, the inhibition of the pump activity by glucose via intracellular signaling (Owada et al., 1999) was implemented ($F_{glc}$; Eq. S55). The amplitude factor of $I_{NaK}$ ($P_{NaK}$) was determined to satisfy $Na^+$ homeostasis in both quiescent and bursting activities. Finally, the $K^+$ balance between efflux through $K^+$ channels and the active influx via NaK was calculated, rather than fixing $[K^+]_i$ as in the original FP model.

### Modeling intracellular $Ca^{2+}$ dynamics

A precise description of ER $Ca^{2+}$ dynamics is critical for modeling β-cell function. Uptake of $Ca^{2+}$ into the ER is mediated by ER $Ca^{2+}$ ATPase (SERCA), and approximately equal amounts of SERCA 2b and 3 are expressed in pancreatic islets (Váradi et al., 1996). The apparent affinity for cytosolic $Ca^{2+}$ was determined with a half-activation concentration ($K_{1/2}$) of 0.27 and 1.1 μM, and a Hill coefficient ($n^H$) of 1.7 and 1.8 for SERCA 2b and 3, respectively (Lytton et al., 1992). The SERCA activity in the present study was represented with a Hill equation of $K_{1/2} = 0.5$ μM and $n^H = 2$, compromised for the whole cell simulation (Eq. S96). $Ca^{2+}$ release from ER is a critical determinant for reconstructing the slow decay phase of $[Ca^{2+}]_i$ observed after action potential burst. Although an application of $IP_3$ facilitates $Ca^{2+}$ release (Tengholm et al., 2001), the slow $Ca^{2+}$ decay during the interburst did not seem to be triggered by $IP_3$-, depolarization-, nor $Ca^{2+}$-induced $Ca^{2+}$ release (Gilon et al., 1999). Therefore, ER $Ca^{2+}$ release ($J_{rel}$) was described as a passive flux down a concentration gradient in this study (Eq. S97).

ER volume ($vol_{ER}$), maximum velocity of SERCA ($P_{SERCA}$; Eq. S96), nor the permeability of the $Ca^{2+}$ release channel ($P_{rel}$; Eq. S97) has been fully measured to provide definite values of these parameters. Thus, they were adjusted based on the following experimental findings. (a) The physiological level of $[Ca^{2+}]_i$ hardly exceeds 0.5 μM during glucose stimulation (Rorsman et al., 1984). (b) The resting $[Ca^{2+}]_i$ is 60–100 nM (Rorsman et al., 1992; Chow et al., 1995). (c) Onset and offset time courses of $Ca^{2+}$ transient were recorded, which were evoked by the action potential burst, a voltage-clamp pulse, or $K^+$-induced depolarization (Gall et al., 1999; Gilon et al., 1999). (d) Direct measurement of $[Ca^{2+}]_{ER}$ using a low affinity $Ca^{2+}$ fluorescent dye revealed that $[Ca^{2+}]_{ER}$ is maximally increased up to ~200 μM by $Ca^{2+}$ uptake through SERCA in the absence of $IP_3$ (Tengholm et al., 2001). It was consistent with $[Ca^{2+}]_{ER}$ of 60–200 μM suggested previously (Tse et al., 1994). (e) At 12 mM [G], $Ca^{2+}$-stimulated ATPase activity of SERCA was comparable to that of PMCA in β cells (Roe et al., 1994). In the present β-cell model, the ratio of ATP consumption by SERCA and PMCA was approximately 1:1 at 12 mM [G], ranging from 1:3 in a quiescent state at 6 mM [G] to 4:3 during continuous firing at 20 mM [G].

### Modeling energy metabolism

Fridlyand et al. (2005) elaborated a set of equations for ATP production through glycolysis and oxidative phosphorylation, and for ATP consumption based on a wide range of biochemical studies. We used their model with a few modifications as follows. First, we changed the glucose dependency of glycolysis ($f_{glc}$) (Eq. S100) to reproduce the experimental finding that the burst duration is prolonged with increasing [G] in β cells. Our revision might be appropriate because $f_{glc}$ reflects the [G] dependency of all the reaction steps including glycolysis and TCA cycle in our model. Note that the original values in the FP model were determined under the assumption that glucose phosphorylation by glucokinase was the only limiting step in glycolysis. Second, we calculated ATP production via β oxidation of fatty acid ($J_{\beta,ox}$; Eq. S99), in addition to glycolysis ($J_{glc}$; Eq. S98). This modification prevented the system from a metabolic collapse at a low [G] (<2 mM), which actually occurred in the FP model. Third, in the production of reduced metabolic compounds (Re), we took account of the total amount of pyridine nucleotides ([$Re_{tot}$]) by adding a term of ([$Re_{tot}$] − [Re]) in $J_{glc}$ and $J_{\beta,ox}$ (Eqs. S98 and S99). This term was crucial to avoid an unlimited increase of [Re] at a high [G] (>15 mM), observed in the FP model. Under the assumption that most Re consists of NADH in the mitochondria, [$Re_{tot}$] of 10 mM was used (Cortassa et al., 2003). The consumption of [Re] by oxidative phosphorylation was calculated using a stoichiometry of 2.5 between ATP and NADH, and with a volume ratio (2.5) between the cytosol and mitochondria (Eq. S102).

### Lead potential ($V_L$) analysis

To clarify the ionic mechanisms underlying burst–interburst rhythm in our new β-cell model, we applied the $V_L$ analysis developed by Cha et al. (2009). The method quantifies the contributions of individual membrane currents to changes in $V_m$ by calculating an equilibrium potential at each moment ($V_L$) using the time-varying conductance ($G_X$), reversal potential ($E_X$), and V-independent transporter current ($I_Y$),

$$V_L = \frac{\sum_X G_X E_X - \sum_Y I_Y}{\sum_X G_X}. \quad (1)$$

Also refer to Eq. S108. $V_L$ always moves in advance of $V_m$, and its time derivative ($dV_L/dt$) drives the automatic change of $V_m$. The relative contribution ($r_c$) of a current component of interest ($i$) is defined by a relative change in $dV_L/dt$ when the time-dependent change of $i$ is selectively fixed. The total sum of $r_c$ for all components equals unity at each time point, and is used to validate the calculations,

$$r_{c,i} = \frac{\frac{dV_L}{dt} - \frac{dV_{L\_Fix,i}}{dt}}{\frac{dV_L}{dt}} \text{ and } \sum_i r_{c,i} = 1. \quad (2)$$

This method has been verified in various cardiac cell models (Cha et al., 2009; Himeno et al., 2011). In the present study, the contribution $c$ (mV $s^{-1}$) was used, instead of $r_c$. $c$ was newly defined by the following equation:

$$c_i = \frac{dV_L}{dt} - \frac{dV_{L\_Fix,i}}{dt} \text{ and } \sum_i c_i = \frac{dV_L}{dt}. \quad (3)$$

$c$ with a positive sign indicates that the corresponding component contributes to membrane depolarization, and vice versa.

Among the three electrogenic ion transporters, V-independent $I_{PMCA}$ was treated as a current source (Eq. S108). $I_{NaK}$ and $I_{NaCa}$ were expressed with Eqs. 4 and 5, where $G_{NaK}$ and $G_{NaCa}$ are the slopes of tangential lines fitted to the instantaneous I-V relation at each moment, and $E_{x\_NaK}$ and $E_{x\_NaCa}$, the intersections of the tangential lines with the x axis:

$$I_{NaK} = G_{NaK}(V_m - E_{x\_NaK}) \quad (4)$$

$$I_{NaCa} = G_{NaCa}(V_m - E_{x\_NaCa}). \quad (5)$$

The contribution of $I_{NaK}$ or $I_{NaCa}$ in Fig. 5 was a summation of $c$ evaluated by fixing $G_{NaK}$ and $E_{x\_NaK}$, or $G_{NaCa}$ and $E_{x\_NaCa}$, respectively. Because $G_{NaK}$ and $E_{x\_NaK}$ are functions of $[Na^+]_i$, $[K^+]_i$, [ATP] or [MgADP], and $V_m$, the contribution of each concentration change was also evaluated in the bottom panels of Fig. 5.

### Online supplemental material

Equations, parameters, and the definition of symbols of the β-cell model are provided in the supplemental material. Table S1 lists the initial values of the 18 variables in this model. Figs. S1 and S2 show reconstructions of $I_{CaV}$ and $I_{KDr}$ in voltage-clamp experiments, respectively. Fig. S3 shows the effect of thapsigargin on the $Ca^{2+}$ transients induced by applying high $K^+$ pulses to the model. Fig. S4 is $V_L$ diagram of the FP model for comparison to our model (Fig. 5). The supplemental material is available at http://www.jgp.org/cgi/content/full/jgp.201110611/DC1.

## RESULTS

### Electrical activity and intracellular concentrations of ions and metabolites in pancreatic β cells

*Burst of action potentials evoked by various glucose concentrations.* Fig. 2 shows the time-dependent changes in $V_m$, [ATP], [MgADP], $[Na^+]_i$, and $[Ca^{2+}]_i$ evoked by different [G] in the new β-cell model. At [G] < 6 mM, the membrane was quiescent, and the concentrations of intracellular ions and metabolites remained at various steady-state levels depending on [G]. The resting potential decreased from −70 mV at 0 mM [G] (not depicted) to −58 mV at 6 mM [G], accompanied by an increase in the input impedance from 4 to 15 GΩ. This input impedance is comparable to experimental measurements of 3–30 GΩ (Rorsman and Trube, 1986), 1–10 GΩ (Rorsman et al., 1986), or 3 GΩ (Smith et al., 1990a). In the simulation, the increase in input impedance largely resulted from the progressive closure of $I_{KATP}$ channels. At 7 mM [G], a typical burst of action potentials appeared. The burst duration was elongated as [G] increased, and finally the burst was transformed to a continuous firing at [G] > 19 mM (Ashcroft et al., 1984; Henquin and Meissner, 1984b). The interburst phase is also elongated at a higher [G] in the present study because more time was required to recover from ion accumulation during the preceding burst period of longer duration. This simulation result is in agreement with the experimental data from mouse islets showing longer burst and interburst periods at a higher [G] (Antunes et al., 2000). Our model, however, failed to reconstruct gradual shortening of the interburst period with [G] (Meissner and Schmelz, 1974).

The action potential in the model is in good agreement with the representative burst activity recorded in a single β cell in the presence of 2.6 mM $[Ca^{2+}]_o$ and 10 mM [G] at 31°C (see Fig. 1 B in Smith et al., 1990a). The maximum rate of rise was 2–3 V $s^{-1}$ in the model, comparable to 3.2 V $s^{-1}$ (Rorsman and Trube, 1986) or 3.5 V $s^{-1}$ (Dean et al., 1975). The peak potential was about −4 mV in the model versus −8.3 mV experimentally (Smith et al., 1990a), the plateau potential was about −50 versus −53.7 mV, and the maximum negative potential during the interburst period was about −68 versus −76.4 mV. The maintenance of the plateau potential was mainly attributable to $I_{CaV}$ conductance remaining at the end of the action potentials. It was supported by a simulation showing that the burst was interrupted if $I_{CaV}$ was instantaneously deactivated by applying a brief hyperpolarizing voltage pulse (not depicted). The $Ca^{2+}$-activated inward currents, $I_{TRPM}$ and $I_{NaCa}$, also contributed to the maintenance of the plateau potential.

*Slow fluctuations in [ATP], [MgADP], $[Na^+]_i$, and $[Ca^{2+}]_i$ during burst–interburst rhythm.* In our model, [ATP] and [MgADP] changed in synchrony with electrical events at [G] > 7 mM (Fig. 2, second row). That is, [MgADP] increased at the expense of ATP during the burst and in turn decreased during the subsequent quiescent period when the cell was relieved from the extra $Ca^{2+}$-dependent ATP consumption. These typical responses were observed at 8 mM [G]. At 12 or 16 mM [G], however, the ATP consumption was compensated for to a greater extent by increased ATP production. Thus, [MgADP] increased much slower during the burst, and its maximum level at the end of burst was lower in spite of the elongated burst duration. On the other hand, the fluctuation in $[Na^+]_i$ was enlarged with an increase in burst duration, and finally $[Na^+]_i$ remained elevated at [G] > 19 mM (Fig. 2). Accumulation of $[Na^+]_i$ was mostly a result of $Na^+$ influx through NCX, which compensated for the large $Ca^{2+}$ influx through $I_{CaV}$. Based on the opposite changes in the fluctuations of [ATP] and $[Na^+]_i$ by increasing [G], our β-cell model predicted that the activation of $I_{NaK}$ by the accumulation of $[Na^+]_i$ might take over the role of $I_{KATP}$ in terminating the burst at a higher [G].

Fluctuation in $[Ca^{2+}]_i$ during the burst–interburst rhythm also has profound effects on the electrical activity. As demonstrated in Fig. 2, $[Ca^{2+}]_i$ jumped from a resting level of ~100 to ~400 nM at the onset of the burst, and then the plateau level of the oscillation (fast $Ca^{2+}$ ripple) slowly decreased during the burst, because of the slow inactivation of $I_{CaV}$. At [G] > 12 mM, a brief oscillation in the plateau level of the $Ca^{2+}$ ripple preceded the final termination of the burst, which has not been described by experimental studies. We found that this oscillation was sensitive to the amplitude of $I_{KCa(SK)}$ but failed to clarify the underlying mechanisms in the present study. After cessation of the burst, a slow decay

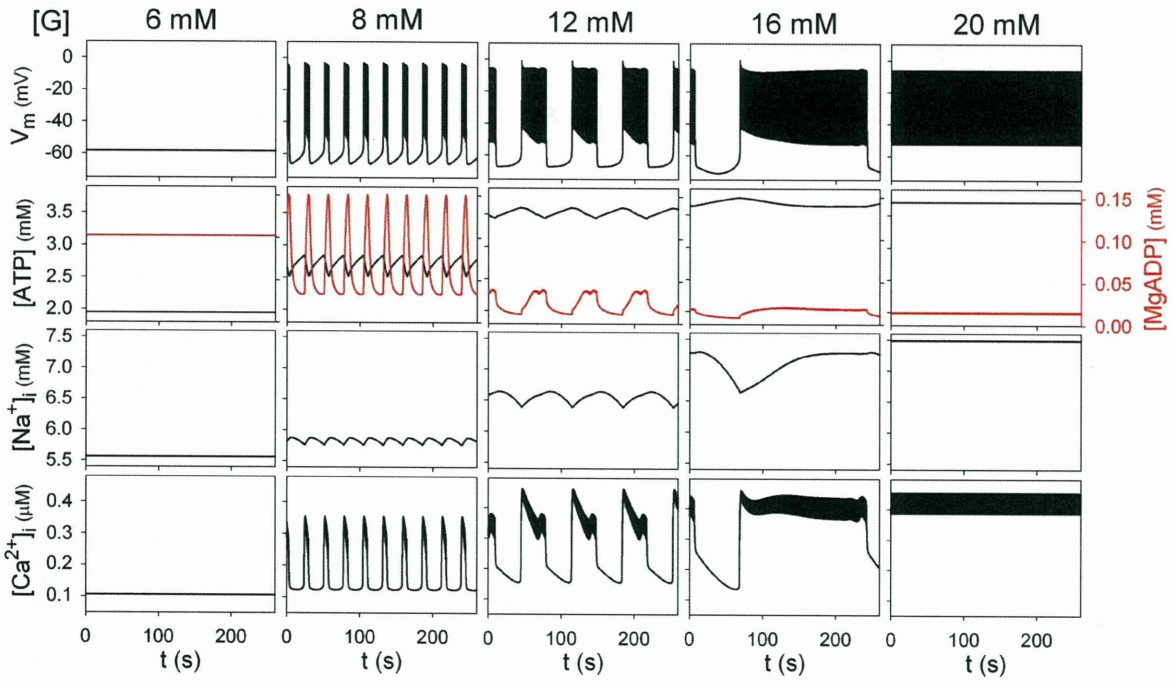


**Figure 2.** Activities of the β-cell model at various [G]. Each row indicates steady cyclic changes in $V_m$, [ATP] (black), [MgADP] (red), $[Na^+]_i$, and $[Ca^{2+}]_i$ in the presence of 8, 12, and 16 mM [G], or a quiescent state at 6 mM [G] and continuous firing of the action potentials at 20 mM [G]. All records were obtained with initial values in Table S1 after the rhythm of the cyclic events became stable after switching [G].

phase (or $Ca^{2+}$ tail) was observed at 12 and 16 mM [G], but hardly at 8 mM [G]. This $Ca^{2+}$ tail is caused by release of $Ca^{2+}$ from the ER, which has accumulated during the preceding burst. The increase in the $Ca^{2+}$ fluctuation at a higher [G] has complex influences on membrane ion channels or transporters, that is, activation of outward-going $I_{PMCA}$ or $I_{KCa(SK)}$, as well as inward-going $I_{NaCa}$ or $I_{TRPM}$. The overall effects of $[Ca^{2+}]_i$ will be evaluated mathematically later.

### Role of ER $Ca^{2+}$ dynamics in glucose-induced burst–interburst rhythm

$Ca^{2+}$ dynamics in the new β-cell model were validated before we analyzed the ionic mechanisms. In control conditions, a regular burst–interburst rhythm and the accompanying $Ca^{2+}$ transients were generated with a cycle length of ~40 s at 11 mM [G] (Fig. 3, the left half). At the onset of a burst, most $Ca^{2+}$ influx through $I_{CaV}$ was instantaneously captured by cytosolic $Ca^{2+}$-binding proteins ($f_i$ in Eq. S5). Then, during the initial 1 s of the burst, the $Ca^{2+}$ influx was compensated for by the ER ($J_{SERCA}$-$J_{rel}$; 44%), PMCA (26%), and NCX (34%) (Fig. 3, bottom), which was in good agreement with experimental results (Gall et al., 1999). As the burst progressed, $Ca^{2+}$ gradually accumulated in the ER, and thus the ER $Ca^{2+}$-buffering capacity became less effective because of an increase in $Ca^{2+}$ release from the ER. Importantly, 97% of the $Ca^{2+}$ accumulated during the whole burst was taken up by the ER, and only 3% remained in the cytosol. After cessation of the burst, the accumulated $Ca^{2+}$ in the ER was slowly released into the cytosol (Fig. 3, bottom), which is a main contributor of the long-lasting $Ca^{2+}$ tail. This simulation result is in line with experimental responses (Gilon et al., 1999).

For further examination of the relevance of the $Ca^{2+}$ dynamics in the model, the effects of blocking SERCA by thapsigargin were simulated. In the right half of Fig. 3 indicated by a gray horizontal bar, the activity of SERCA was reduced to 20% of the control. As a result, the $Ca^{2+}$-buffering capacity of ER decreased, and in the steady state, the amplitude of $Ca^{2+}$ oscillation was increased by nearly two times. In addition, the $Ca^{2+}$ tail disappeared from the interburst period and the electrical rhythm became about two times faster through the shortening of both interburst and burst periods. These findings are in good agreement with several experimental recordings (Miura et al., 1997; Gilon et al., 1999; Fridlyand et al., 2003) and previous simulation results (Fridlyand et al., 2003; Bertram and Sherman, 2004). The rate of depolarization during the interburst was accelerated by the activation of inward $I_{SOC}$ as a result of ER depletion. The burst duration was also reduced because the opening of $I_{KATP}$ was accelerated by the enhanced $Ca^{2+}$-dependent ATP consumption. Increased outward $I_{KCa(SK)}$ or $I_{PMCA}$ by the amplified $Ca^{2+}$ transient might also help the early termination of the burst, whereas inward $I_{NaCa}$ and $I_{TRPM}$ have the opposite effects.

We also simulated $Ca^{2+}$ transients induced by applying 45 mM of $K^+$ solution (Fig. S3). The $Ca^{2+}$ tail observed after the high $K^+$ pulse was well reconstructed (Gilon et al., 1999). The simulation predicted that $[Ca^{2+}]_{ER}$ was accumulated up to ~60 μM via $I_{CaV}$ activated through high $K^+$-induced depolarization (approximately −25 mV). In the presence of thapsigargin, the amplitude of $Ca^{2+}$ transients was increased with a large initial peak, and the slow $Ca^{2+}$ tail disappeared. The slow inactivation of $I_{CaV}$ caused the marked decrease in $[Ca^{2+}]_i$ during the initial 10 s of the pulse, as well as the temporal depression after washing out the high $K^+$ solution.

### Ionic mechanisms underlying the electrical activity of β cells

*Current profile during the burst and interburst periods.* The findings in Fig. 2 suggested that the burst rhythm is determined by the balance among current components

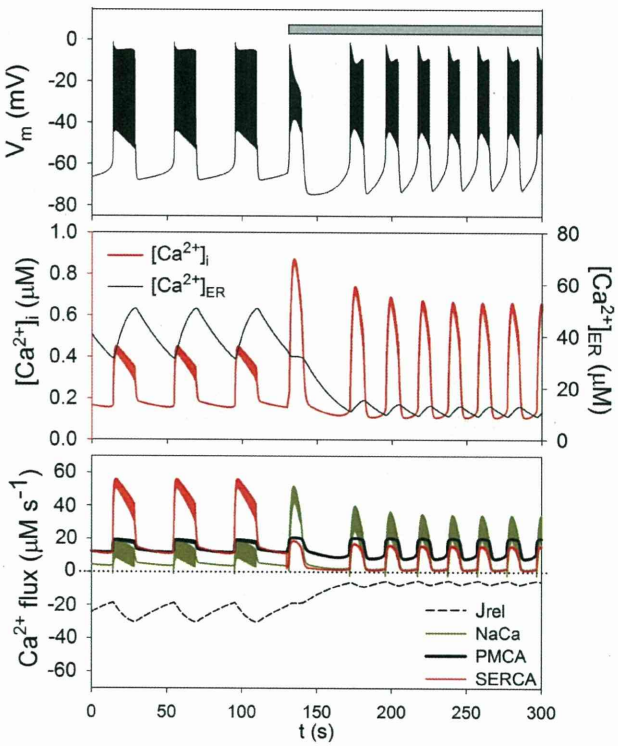


**Figure 3.** Dynamics underlying spontaneous $Ca^{2+}$ oscillations before and after inhibition of SERCA. Time-dependent changes in $V_m$ (top), and $[Ca^{2+}]_i$ and $[Ca^{2+}]_{ER}$ (middle), and $Ca^{2+}$ fluxes through $J_{rel}$, $J_{SERCA}$, $I_{NaCa}$, and $I_{PMCA}$ (bottom) at 11 mM [G] are illustrated with different colors, as indicated in each panel. The scale of $[Ca^{2+}]_{ER}$ is represented on the right y axis (middle), and the zero flux level is indicated by a dotted line (bottom). From 130 s (gray horizontal bar), $P_{SERCA}$ was reduced to 20% of its control value (from 0.096 to 0.0192 amole $ms^{-1}$) to simulate the blocking effect of SERCA by thapsigargin. The net $Ca^{2+}$ flux through the ER was calculated by subtracting $J_{rel}$ from $J_{SERCA}$.

that are modulated by slow changes in [ATP] and [MgADP], as well as those in $[Na^+]_i$ and $[Ca^{2+}]_i$. We measured the amplitudes of all these currents, including $I_{KATP}$, $I_{NaK}$, $I_{NaCa}$, $I_{PMCA}$, $I_{TRPM}$, and $I_{KCa(SK)}$, at 8 and 16 mM [G], in addition to V-dependent $I_{CaV}$ and $I_{KDr}$ (Fig. 4). During the burst period, the current levels were measured at the most negative potential between successive action potentials. The plateau potential gradually shifted negative toward the threshold for the full repolarization of the burst termination. At both [G], $I_{KDr}$ was of minimum size because of almost complete deactivation at the end of individual action potentials, and its contribution to changing the plateau potential seemed to be negligible. In contrast, $I_{CaV}$ had the largest amplitude, suggesting that it is the major current maintaining the plateau potential or driving the interburst depolarization to trigger the subsequent action potential burst. $I_{KATP}$ provided a sizable outward current during the interburst at 8 mM [G] but was much decreased at 16 mM [G]. In contrast, outward $I_{NaK}$ and $I_{KCa(SK)}$, and inward $I_{NaCa}$ and $I_{TRPM}$, were substantially increased at 16 mM [G] by the accumulation of $[Na^+]_i$ and $[Ca^{2+}]_i$ during the prolonged burst period. The amplitude of $I_{SOC}$ was negligibly small throughout the records in Fig. 4 at both 8 and 16 mM [G] (not depicted). These current profiles, however, only give clues as to the contribution of individual currents underlying the generation of electrical bursting activity. A quantitative understanding of the ionic mechanisms requires further mathematical analysis, such as $V_L$ analysis in the next section or bifurcation analysis as described in our companion paper (see Cha et al. in this issue).

*$V_L$ analysis of interburst ionic mechanisms.* To measure the contribution of each current component to automatic change in $V_m$, $V_L$ analysis was applied to the simulation results (Eqs. 1, 3, and S108). The magnitudes of the contribution ($c$ in mV $s^{-1}$; see Materials and methods) of individual ion channels and transporters were calculated over the interburst period, as indicated with horizontal gray bars in Fig. 4 (A and B). $c$ was plotted in a cumulative manner at 8 and 16 mM [G] (Fig. 5, middle panels).

At 8 mM [G], V-dependent activation of $I_{CaV}$ ($d_{CaV}$), albeit a tiny change from 0.03 to 0.05, provided the largest positive contribution during the entire course of slow depolarization (Fig. 5 A). In contrast, the contribution of ultraslow inactivation of $I_{CaV}$ ($f_{us}$) was trivial. $I_{KATP}$, an outward current, also provided a positive contribution to the depolarization ($c \sim 0.1$–$0.2$ mV $s^{-1}$) because its open probability was gradually reduced by both increasing [ATP] and decreasing [MgADP]. In the late phase, the contribution of $I_{KATP}$ became smaller by gradual equilibration of [ATP] and [MgADP]. The positive contribution of inward $I_{NaCa}$ ($c < 0.1$ mV $s^{-1}$) was mainly attributable to increased turnover rate by the gradual decrease of $[Na^+]_i$ after cessation of the burst. $I_{NaK}$, $I_{KCa(BK)}$, and $I_{TRPM}$ hindered the slow depolarization, as

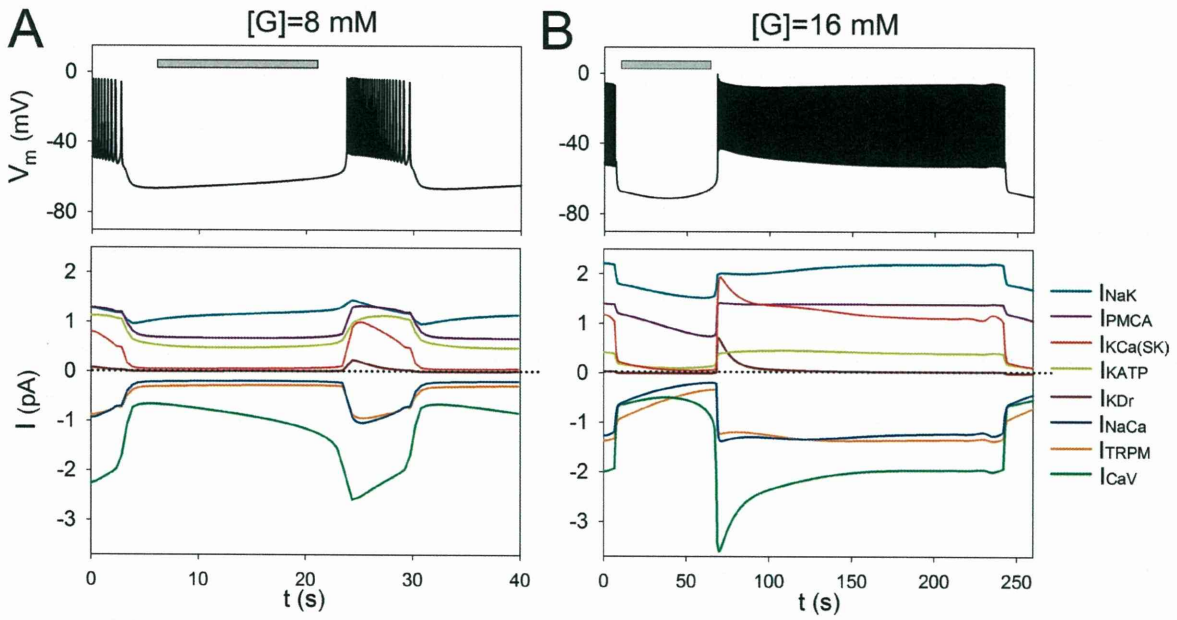


**Figure 4.** Ionic currents during burst and interburst activity at 8 mM [G] (A) and 16 mM [G] (B). Top panels show $V_m$ and bottom panels show individual ionic currents, with the different colors as indicated on the right. The amplitudes of individual currents were measured at the plateau potential (the most negative potential between successive action potentials) during the burst period. Note that different time scales are used in A and B. The zero current level is indicated by dotted lines. Gray bars indicate the interburst period, where the $V_L$ analysis was applied in Fig. 5.

represented by their negative contributions (less than $-0.2$ mV $s^{-1}$).

At 16 mM [G], the ionic mechanisms changed markedly (Fig. 5 B). The contribution of $I_{KATP}$ almost disappeared from the $V_L$ diagram, but the contribution of $Ca^{2+}$-dependent currents ($I_{PMCA}$, $I_{NaCa}$, and $I_{TRPM}$) noticeably increased in compared with those at 8 mM [G]. The $V_m$ change showed two phases during the interburst period: early hyperpolarization and late depolarization. During the early phase, the hyperpolarization was mainly attributed to decreases in inward $I_{NaCa}$ and $I_{TRPM}$ as a result of the slow decay of $[Ca^{2+}]_i$. The sum of these hyperpolarizing effects was larger than the depolarizing effect caused by the decrease in outward $I_{PMCA}$. In the late phase, the decay rate of $[Ca^{2+}]_i$ slowed down, the contribution of $I_{NaCa}$ was reversed by the decrease in $[Na^+]_i$, and the negative contribution of $I_{TRPM}$ was also reduced. Furthermore, the decrease in $[Na^+]_i$ gradually reduced outward $I_{NaK}$ and contributed to depolarization. As a consequence, the membrane started to depolarize at the late phase.

Comparison of the $V_L$ diagrams in Fig. 5 (A and B) reveals that a metabolic-dependent mechanism ($I_{KATP}$) at a lower [G] was replaced by an ion-dependent mechanism ($I_{PMCA}$, $I_{NaCa}$, and $I_{TRPM}$) at a higher [G] in generating the burst–interburst rhythm. This replacement of mechanism was further exemplified by separating the contribution of $I_{NaK}$ into metabolism- and ion-dependent mechanisms (Fig. 5, bottom panels). At 8 mM [G], a negative contribution of $I_{NaK}$ was caused by rapid recovery of the ATP/MgADP composition, whereas at 16 mM [G], the metabolic effects almost disappeared, and the decrease in $[Na^+]_i$ dominated the time course of $c$ of $I_{NaK}$.

*$V_L$ analysis of repetitive action potentials.* The result of $V_L$ analysis is presented in Fig. 6 for two successive action potentials during the burst. The $V_L$ (Fig. 6, red line) leads the time-dependent change in $V_m$ (black line) in advance and intersects the $V_m$ curve when $dV_m/dt$ (or $I_{tot}$) equals zero. The $V_L$ diagram (Fig. 6, bottom) indicates that the time course of the action potential is largely determined by $I_{CaV}$. In the rising phase of the spontaneous action potential, the progressive V-dependent activation of $I_{CaV}$ plays the major role; likewise, the V-dependent deactivation of $I_{CaV}$ is mainly responsible for repolarization. The activation of $I_{KCa(BK)}$ partially counteracts $I_{CaV}$ to reduce the maximum rate of rise or decay of the action potential. Surprisingly, the delayed activation of outward $I_{KDr}$ provided a negative contribution only at the beginning of the repolarizing phase, but then reversed its contribution to retard the repolarizing influence of $I_{CaV}$. This retarding effect of $I_{KDr}$ is a result of V-dependent removal of activation ($p_{KDr}$). The contributions of the other substrate-dependent currents, $I_{KATP}$, $I_{PMCA}$, $I_{NaCa}$, $I_{TRPM}$, and $I_{NaK}$, are barely

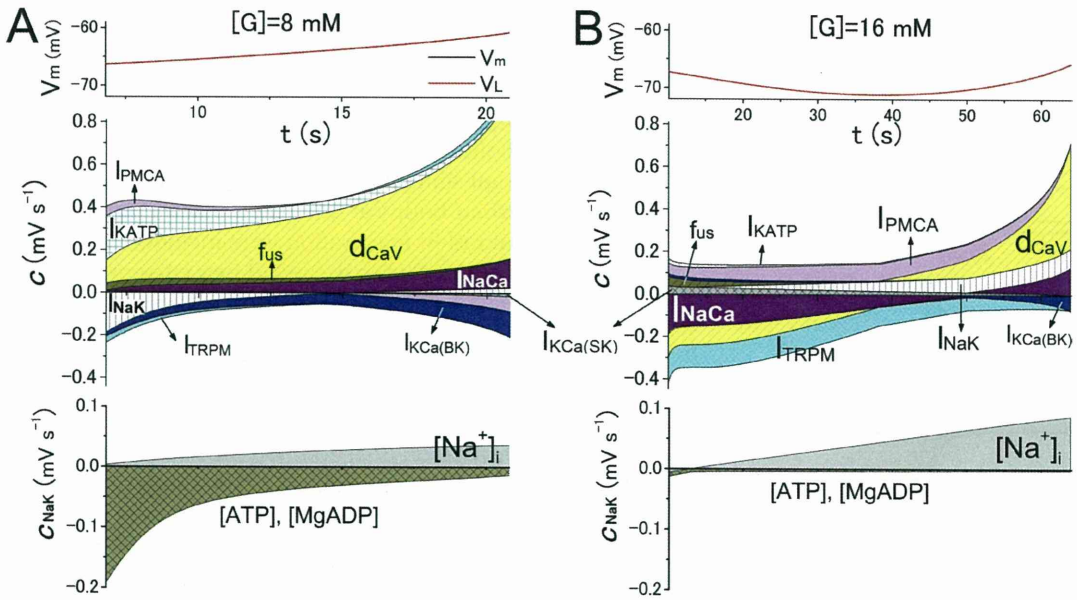


**Figure 5.** $V_L$ diagrams show the contribution of major currents during the interburst period at 8 mM [G] (A) and 16 mM [G] (B). (Top) Time-dependent changes in $V_L$ (red) and $V_m$ (black). The $V_m$ trace is overlapped by $V_L$. (Middle) Time-dependent changes in the contribution ($c$) of individual currents indicated with different colors. A positive $c$ indicates that the time-dependent change in the corresponding current contributes to depolarization (in mV $s^{-1}$), and vice versa. The contribution of $I_{CaV}$ was divided into $c$ of $d_{CaV}$ and $c$ of $f_{us}$. The rest for $I_{CaV}$ was negligibly small (not depicted). (Bottom) Separation of the contribution of $I_{NaK}$ into [ATP]- and [MgADP]-dependent components (dark yellow) and $[Na^+]_i$-dependent component (gray). Effects of other factors on $I_{NaK}$, such as time-dependent changes in $[K^+]_i$ or $V_m$, were negligibly small (not depicted). The time scales refer to those for the gray bars in Fig. 4 (A and B).

visible because the concentrations of ions or metabolites changed minimally over the time span of an action potential.

### An extra effect of [G] on the bursting activity through direct inhibition of NaK

Owada et al. (1999) demonstrated that applying glucose to β cells inhibited $Na^+/K^+$ ATPase in a dose-dependent and reversible manner via a distinct signal transduction pathway. Because this inhibition was of considerable magnitude (up to 55%), they suggested that the inhibition of $I_{NaK}$ might promote insulin secretion at a high [G]. We tested this hypothesis by switching on the inhibitory action of glucose on $I_{NaK}$ ($F_{glc}$; Eq. S55) after a steady rhythm was established (Fig. 7). Immediately after $I_{NaK}$ was reduced by introducing the glucose inhibition (Fig. 7, gray bar), an action potential burst of longer duration was evoked accompanied by a larger $Ca^{2+}$ transient, in agreement with the experimental observations using an NaK blocker (Bozem and Henquin, 1988). Contrary to the expectation of Owada et al. (1999), the burst interval returned to control at the next burst and remained constant. The amplitude of $I_{NaK}$ was almost restored because $[Na^+]_i$ gradually increased until $I_{NaK}$ exactly matched the $Na^+$ influx. The basal level of $[Ca^{2+}]_i$ was initially increased by the intervention but slowly recovered over the next 100 s. Similar results were simulated at 12 mM [G]. The simulation suggests that the partial inhibition of $I_{NaK}$ by glucose might increase insulin secretion at 8 mM [G], but the effect is only transitory.

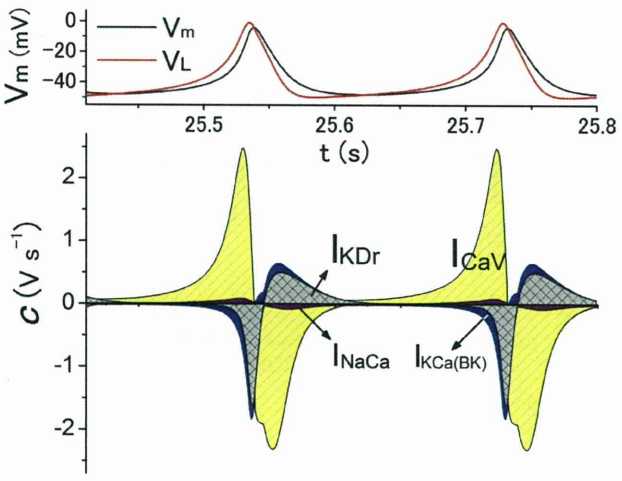


**Figure 6.** $V_L$ diagram for two successive action potentials within the burst at 8 mM [G]. (Top) Time-dependent changes of $V_L$ (red) and $V_m$ (black). Note that $V_L$ always changes in advance of $V_m$. (Bottom) Time-dependent changes in contributions ($c$) of $I_{CaV}$, $I_{KDr}$, $I_{KCa(BK)}$, and $I_{NaCa}$. The $c$ of other currents was also plotted in the diagram but is barely visible because of its minor contributions. The time scale on the x axis refers to that in Fig. 4 A.

## DISCUSSION

By integrating a broad range of electrophysiological findings into a mathematical model, the response of pancreatic β cells to extracellular glucose was well reconstructed, and the underlying mechanisms were elucidated in a comprehensive manner. The new β-cell model showed a series of responses to varying [G], that is, the intermittent burst of action potentials accompanied by $Ca^{2+}$ transients at [G] > 7 mM, the elongation of the burst duration with increasing [G], and the continuous firing of action potentials at [G] > 19 mM. $V_L$ analysis of the model successfully quantified contributions of ion channels and transporters to the slow interburst depolarization. It was concluded that alternating burst and interburst events at the physiological range of [G] is regulated mainly by $I_{KATP}$ channels, which transduce signals from varying [ATP] or [MgADP] to membrane excitability. The novel prediction is that the role of $I_{KATP}$ is taken over by electrogenic ion transporters, such as $I_{NaCa}$, $I_{NaK}$, $I_{PMCA}$, and a $Ca^{2+}$-activated ion channel, $I_{TRPM}$, at a higher [G].

### Comparison with the FP model

To our knowledge, the β-cell model developed by Fridlyand et al. (2003, 2005) provided the first description of individual channels and transporters on a plasma membrane at a molecular level. Our model is based on the structure of this FP model to couple membrane excitation with energy metabolism. We revised most of the ionic current components with reference to more extensive electrophysiological findings. In the FP model, a high $K^+$ external solution induces continuous $Ca^{2+}$ influx through $I_{CaV}$ (about −30 to −50 pA) and eventually causes a metabolic collapse by a rapid depletion of cytosolic ATP. Relevant simulations to experimental findings were obtained when both $Ca^{2+}$-mediated inactivation and V-dependent ultraslow inactivation were included in the new model of $I_{CaV}$. Moreover, we added new currents, $I_{TRPM}$ and $I_{KCa(BK)}$, based on recent experimental findings. We found that $I_{TRPM}$ is an important current to maintain the plateau potential around −50 mV during an action potential burst, whereas a full repolarization between action potentials was observed in the FP model. $I_{KCa(BK)}$ is important in the regulation of action potential amplitude.

For self-consistency of the model, we included all ion transports across the cell membrane in calculating both $V_m$ and intracellular ion concentrations, according to charge conservation law (see Cha et al., 2011). (a) We took account of the $H^+$ influx via $Ca^{2+}/H^+$ exchange through PMCA. This $H^+$ flux was assumed to be completely converted to equivalent $Na^+$ flux by a fast $Na^+/H^+$ exchange (see Materials and methods). (b) $[K^+]_i$ was not fixed in our model, but the time-dependent change was calculated by $K^+$ fluxes through NaK and ion channels. These modifications were prerequisite for examining

the roles of ion transporters, which are greatly affected by ion concentrations.

The model of $I_{NaK}$ in the FP model was largely modified from the original model of Chapman et al. (1983) by omitting state transitions of the carrier protein. This simplification resulted in no saturation of the turnover rate by $[Na^+]_i$. Moreover, $I_{NaK}$ in the FP model is a V-independent current in the range from −80 to 0 mV. We implemented a new kinetic model of $I_{NaK}$ with the state transitions (Oka et al., 2010). It shows properties well established in experimental studies, such as dependencies on $Na^+$ and $K^+$, the free energy of ATP hydrolysis ($\Delta G_{ATP}$), and the membrane potential. Thereby, the present study reliably predicted that $I_{NaK}$ took a pivotal role in terminating the burst when $[Na^+]_i$ was accumulated during a long-lasting burst at a high [G] (Fig. 5). For comparison with the present study, we applied $V_L$ analysis to the slow interburst depolarization in the FP model (Fig. S4). At a relatively low [G] (8.5 mM), a $V_L$ diagram demonstrated that the time-dependent decrease of outward $I_{NaK}$ takes the major role in determining the depolarization rate ($c \sim 0.25$ mV $s^{-1}$), whereas the contribution of $I_{KATP}$ was negligibly small ($c \sim 0.025$ mV $s^{-1}$). It is because of a relatively rapid production of ATP in the FP model, resulting in a long-lasting burst even at relatively lower [G], accompanied by $[Na^+]_i$ oscillation with an amplitude of ~2 mM.

### Mechanisms to generate the bursting activity in modeling studies

Complex patterns of electrical activity in β cells with varying [G] has been one of the interesting targets in the field of mathematical physiology, and several explicit hypotheses have been put forward in various forms of mathematical models. Importantly, however, the fundamental question still remained as to what the slowly varying factor underlying the time course of burst–interburst rhythm in β cells is. Here, we discuss the multiple key membrane components suggested in relation to the slow intracellular factors hypothesized in previous modeling studies, that is, $[Ca^{2+}]_i$, $[Ca^{2+}]_{ER}$, [ATP] and/or [ADP], and $[Na^+]_i$.

*$[Ca^{2+}]$ and the $Ca^{2+}$-activated $K^+$ currents.* One of the major hypotheses assumed a gradual activation of $Ca^{2+}$-dependent $K^+$ currents during an action potential burst. For example, early Chay-Keizer models adopted the BK channel (Chay and Keizer, 1983; Sherman et al., 1988), and they predicted that an accumulation of intracellular $Ca^{2+}$ via repetitive spikes increased the outward BK current and terminated the burst. In turn, the burst was resumed when the BK channels were sufficiently deactivated during the interburst period. Distinct from the expectation in their models, however, the progressive accumulation of $Ca^{2+}$ has not been established experimentally, but rather, a rapid rise of the $Ca^{2+}$ transient leveled off to the plateau level within the initial several seconds of the burst (Santos et al., 1991; Worley et al., 1994a), or $[Ca^{2+}]_i$ slightly rose (Gilon and Henquin, 1992; Zhang et al., 2003) or decayed (Miura et al., 1997; Henquin et al., 2009; Merrins et al., 2010) thereafter. In recent studies, an existence of a different type of $Ca^{2+}$-dependent $K^+$ channel, $I_{Kslow}$, has been reported (Göpel et al., 1999a; Goforth et al., 2002; Zhang et al., 2005).

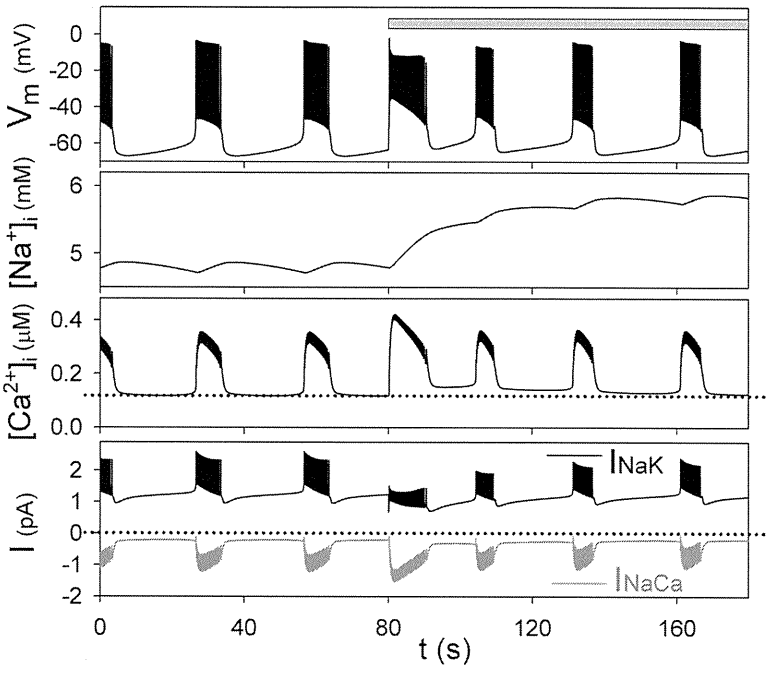


**Figure 7.** Effects of the inhibition of $Na^+/K^+$ ATPase by glucose. The inhibition of NaK by glucose was introduced from 80 s (gray bar) by changing $F_{glu}$ (Eq. S55) from 1 to 0.552 at 8 mM [G]. The panels show time courses of $V_m$, $[Na^+]_i$, $[Ca^{2+}]_i$, $I_{NaK}$, and $I_{NaCa}$. Dotted lines indicate the initial basal level of $[Ca^{2+}]_i$ (third panel) and zero current levels (bottom panel).

The important role of $I_{Kslow}$ in terminating the burst via $[Ca^{2+}]$ accumulation was suggested by two mathematical models (Goforth et al., 2002; Fridlyand et al., 2009). To simulate the expected slow kinetics of $I_{Kslow}$, Goforth et al. (2002) assumed a localized subspace with a substantial volume (occupying ~30% of the cytosolic volume), in which the $Ca^{2+}$ concentration activating $I_{Kslow}$ varies in parallel to changes in $[Ca^{2+}]_{ER}$, rather than the more rapid variation of $[Ca^{2+}]_i$. However, such kinetic changes in $I_{Kslow}$ during the bursting activity nor any histological evidence to justify the diffusion barrier have been found experimentally. Alternatively, Fridlyand et al. (2010) assumed $I_{KCas}$ with an extremely slow time constant of 2.3 s for activation to represent $I_{Kslow}$. However, SK channels, one of the candidates contributing to the experimental $I_{Kslow}$, show very fast gating kinetics (Hirschberg et al., 1998).

The slow decay phase of $[Ca^{2+}]_i$ after the burst might lead to slow changes in membrane conductances of several $Ca^{2+}$-activated channels or transporters. Indeed, the present study suggests that $[Ca^{2+}]_i$ might play a significant role in driving slow interburst depolarization through $I_{PMCA}$, $I_{NaCa}$, and $I_{TRPM}$, as well as $I_{KCa(SK)}$ (Fig. 5). Unfortunately, only a few indirect measurements of these currents have been reported experimentally. As a result, the contribution of $I_{TRPM}$ was only considered in our model, and $I_{NaCa}$ and $I_{PMCA}$ were implemented in a few previous models (Fridlyand et al., 2003; Diederichs, 2006; Meyer-Hermann, 2007).

*$[Ca^{2+}]_{ER}$ and $I_{SOC}$.* Repetitive empting and refilling of ER is closely related to bursting rhythm by modulating $Ca^{2+}$-activated currents. Among them, a store-operated inward current, $I_{SOC}$ (sometimes termed $I_{CRAC}$ or $I_{CRAN}$), would be a primary candidate to generate the bursting rhythm. Gilon et al. (1999) suggested that ER fills with $Ca^{2+}$ during the burst, and the gradual deactivation of $I_{SOC}$ may lead to termination of the burst. Conversely, the subsequent emptying of the ER after the burst might then reactivate $I_{SOC}$ to trigger a new burst. This mechanism has been tested in several models (Bertram et al., 1995a; Chay, 1996, 1997; Mears et al., 1997; Fridlyand et al., 2003). However, the half-activation concentration of $[Ca^{2+}]_{ER}$ ($K_{0.5,ER}$) has not been measured experimentally, and thus the predicted contributions of $I_{SOC}$ are different among studies. For example, in the models of Chay (1996, 1997) using a $K_{0.5,ER}$ of 50 or 70 μM, the gating of $I_{SOC}$ took a central role in determining the burst rhythm. On the other hand, in the other models $I_{SOC}$ contributed little because the channel remained closed as a result of the assumption of a relatively low $K_{0.5,ER}$ (3 μM; Bertram et al., 1995a, and the present model), or was always open because of an assumed high $K_{0.5,ER}$ (200 μM; Fridlyand et al., 2003). Therefore, it is important for $K_{0.5,ER}$ to be determined experimentally to decide the role of $I_{SOC}$ in generating glucose-induced bursting rhythm under normal conditions. Interestingly, rather consistent effects (the prolongation of the spike burst or the acceleration of the bursting rhythm) were reconstructed with these differing models when $I_{SOC}$ was maximally activated by ER depletion under thapsigargin, muscarinic antagonist, or low glucose (Bertram et al., 1995a; Mears et al., 1997; Fridlyand et al., 2003; the present model).

*[ATP] and [ADP] and $I_{KATP}$.* [ATP] and/or [ADP] have been considered as key slow factors, and several β-cell models examined the time-dependent gating of $K_{ATP}$ channels. However, quantitative estimation of the contribution of $I_{KATP}$ to burst activity is highly dependent on the formulation of both $I_{KATP}$ and the metabolic components of each model. For example, Magnus and Keizer (1998) developed a detailed $I_{KATP}$ model and concluded it was a major factor, whereas simulations using the FP model and the same $I_{KATP}$ formulation concluded that $I_{KATP}$ was not of major significance. This is because the two models adopted radically different schemes describing the production of [ATP] and [MgADP].

In addition, it should be noted that ATP-consuming transporters, such as PMCA, SERCA, and NaK, should influence the bursting rhythm by modulating their activities according to the intracellular energy level. However, few studies have dealt with this subject, except the present model by incorporating the detailed kinetic model of $I_{NaK}$ with $\Delta G_{ATP}$ dependency.

*$[Na^+]_i$ and $I_{NaK}$.* As demonstrated here and in previous modeling studies (Miwa and Imai, 1999; Fridlyand et al., 2003; Meyer-Hermann, 2007), glucose-induced fluctuations of $I_{CaV}$ results in rhythmical $Na^+$ entry through the action of NCX. Increased $[Na^+]_i$ will activate $I_{NaK}$ and lead to termination of the burst; in turn, a slow decay of $[Na^+]_i$ leads to a decrease in $I_{NaK}$ during the interburst period. Experimentally, Grapengiesser (1996, 1998) observed distinct oscillations of $[Na^+]_i$ under a partial suppression of NaK in mouse β cells. In support of this idea, these oscillations disappeared after inhibition of $I_{CaV}$ or under a lower glucose, but they were insensitive to a blocker of V-dependent $Na^+$ channels.

$[Na^+]_i$ also modulates the turnover rate of the NCX exchanger. Thus, a proper $Na^+$ dependency of $I_{NaCa}$ is essential for examination of the role of $[Na^+]_i$ in generating bursting activity. The kinetic scheme of $I_{NaCa}$ used in this study was developed in cardiac cells and has been well tested experimentally. In addition, the tetrodotoxin-sensitive $Na^+$ current ($I_{Na}$) might also contribute to intracellular $Na^+$ accumulation. In preliminary studies, we implemented $I_{Na}$ based on recordings in pancreatic β cells from rat (Hiriart and Matteson, 1988), mouse (Göpel et al., 1999b; Vignali et al., 2006), and human (Braun et al., 2008). However, because $I_{Na}$ was almost completely inactivated at the physiological $V_m$, the

generated flux was trivial. $V_L$ analysis also revealed that $I_{Na}$ made a very minor contribution to the slow depolarization. Thus, $I_{Na}$ was deleted from the present model.

The $[Na^+]_i$ of 10–14 mM recorded by Grapengiesser (1996) is much higher than the 5.5–7.5 mM in our simulations. When examined with our model, however, 10–14 mM $[Na^+]_i$ resulted in the reverse mode of the NCX all through the normal burst activity because the $Na^+$-driving force is much reduced. Furthermore, the amplitude of the oscillation of $[Na^+]_i$ and the corresponding effect on $I_{NaK}$ were reliably estimated in our study. This is because the average $Na^+$ influx through the NCX was determined by the amplitude of $I_{CaV}$ and the action potential frequency, both of which were consistent with experimental data.

### Is a single β cell capable of generating full-sized action potentials?

Remarkably, the action potential parameters in our model are quite comparable to experimental measurements in isolated mouse β cells obtained by Smith et al. (1990a) (see Slow fluctuations in [ATP]... in Results). In most papers, however, the amplitude of action potentials was smaller and the quiescent potential less negative when recorded in single β-cell preparations (Rorsman and Trube, 1986; Santos et al., 1991; Kinard et al., 1999; Bertram et al., 2000). It is conceivable that the action potentials might be damped under the patch-clamp recording because the current leak through the gigaseal (~10 GΩ) between the patch electrode and the cell membrane is comparable to the whole cell membrane current (input resistance of ~10–30 GΩ). The membrane capacitance of ~6 pF of small β cells is also in the same order as the floating capacitance of the electrode tip. Moreover, recovery from dissociation injury might be incomplete in culture medium, or action potential generation might be depressed at room temperature or by the rundown of $I_{CaV}$. It should be noted that mouse or human β cells contain a relatively high density of $I_{CaV}$ ranging over 6 to 11.4 pA $pF^{-1}$, with an apparent reversal potential of ~50 mV at physiological $[Ca^{2+}]_o$ (see Table I for references). The current densities of $I_{CaV}$ guarantee a fast rising phase and a full size of the action potential in an intact cell before patch-clamp recording. In the present model, the action potential peak was shifted to positive potentials when the membrane $K^+$ conductance was partially blocked, in agreement with experiments (Atwater et al., 1979; Santos and Rojas, 1989; Rorsman et al., 1992; Houamed et al., 2010). In addition to the action potential amplitude, it should also be noted that the burst duration in single-cell preparations might be affected by the leak conductance and floating capacitance during patch recordings. The difference between electrical activities in single cells and those of islets might be caused by the above recording artifacts.

### Further considerations and limitations of the study

The $V_L$ diagram in Fig. 5 indicated prominently large contributions of $I_{CaV}$ during the whole interburst period at both 8 and 16 mM [G]. These contributions are mainly attributable to the increase or decrease in $d_{CaV}$, which is a pure voltage-dependent gate of $I_{CaV}$. From the viewpoint that burst–interburst rhythm is principally generated by slow changes in cytosolic substrate concentrations, the role of $d_{CaV}$ is to magnify changes in $V_m$ in the same direction as those induced by other membrane currents under the influence of cytosolic factors. Namely, at 8 mM [G], the slow depolarization induced by changes in $I_{KATP}$ and $I_{NaCa}$ increases $d_{CaV}$, which results in further depolarization. In the early half of the interburst period at 16 mM [G], $d_{CaV}$ is decreased as a result of the negative shift of $V_m$, which is primarily induced by a decrease in $I_{NaCa}$ or $I_{TRPM}$ via the progressive decay of $[Ca^{2+}]_i$. During the late phase, the gradual positive shift in $V_m$ induced by a decrease in $I_{PMCA}$ or $I_{NaK}$ increases $d_{CaV}$ to enhance the depolarization. If these secondary contributions of $I_{CaV}$ are excluded from comparison of the membrane currents, the $V_L$ diagram indicates that $I_{KATP}$ and $I_{NaCa}$ at 8 mM [G], and $I_{NaCa}$, $I_{PMCA}$, $I_{TRPM}$, and $I_{NaK}$ at 16 mM [G], play major roles in converting variations in the slow cytosolic factors into the $V_m$ change in our model.

The effects of thapsigargin on $[Ca^{2+}]_i$ have been examined in several experiments using islet preparations, because blocking the ER might provide important clues as to the role of $Ca^{2+}$ buffering by the ER in the bursting rhythm. Unfortunately, there have been no experimental data showing the effects of thapsigargin on the electrical activity or on $Ca^{2+}$ fluctuations in isolated individual β cells. In our single-cell model, the simulation of applying thapsigarin (Fig. 3) was consistent with the accelerated rhythm of the $Ca^{2+}$ fluctuations recorded in several experimental observations in pancreatic islets (Miura et al., 1997; Gilon et al., 1999; Fridlyand et al., 2003), provided that the rhythm of $Ca^{2+}$ transient reflects the electrical

TABLE I

*Measurements of the peak of $I_{CaV}$*

| Amplitude of $I_{CaV}$ | External solution (mM $Ca^{2+}$) | Species | Reference |
|---|---|---|---|
| 51 pA (8.28 pA $pF^{-1a}$) | 2.6 | mouse | Rorsman et al., 1992 |
| 37 pA (6.00 pA $pF^{-1a}$) | 2.6 | mouse | Islam et al., 1995 |
| 70 pA (11.37 pA $pF^{-1a}$) | 2.6 | mouse | Vignali et al., 2006 |
| 93 pA | 2.6 | mouse | Göpel et al., 1999b |
| 135 pA (21.92 pA $pF^{-1a}$) | 10 | mouse | Gilon et al., 1997 |
| 16 pA $pF^{-1}$ | 10 | mouse | Arkhammar et al., 1994 |
| 16 pA $pF^{-1}$ | 10 | mouse | Ämmälä et al., 1992 |
| 17 pA $pF^{-1}$ | 10.2 | mouse | Bokvist et al., 1991 |
| 6.5 pA $pF^{-1}$ | 5 | human | Kelly et al., 1991 |
| 7 pA $pF^{-1}$ | 2.6 | human | Braun et al., 2008 |

[a]Current density.

bursting activity even in the islet preparations. However, it should be noted that in other islet studies, thapsigargin induced a sustained increase in $[Ca^{2+}]_i$ (Worley et al., 1994b; Gilon et al., 1999; Kanno et al., 2002), accompanied by a continuous firing of action potentials (Worley et al., 1994b). Furthermore, both of these responses have been observed in the same experimental study (Miura et al., 1997). At present, it might be speculated that our cell model represents only a given population of β cells, or that the cell-to-cell electrical coupling among different populations of cell types within the islet can produce different patterns in the thapsigargin response.

Although the current system was much improved compared with the previous β-cell models by adding individual current components in the molecular level, further refinement of the formulation will be necessary according to new experimental data in future, especially in respect to temperature effects on channel kinetics. Furthermore, compared with the electrophysiological formulations, the description of energy metabolism is quite simplified in our β-cell model. Therefore, it is beyond the scope of this study to reproduce an ultraslow bursting rhythm with periods >5 min, which have been suspected to be of metabolic origin (Henquin et al., 1982; Bertram et al., 2004). Moreover, the effect of $[Ca^{2+}]_i$ on ATP production was not considered in our model. Keizer and Magnus (1989) assumed that $Ca^{2+}$ entry into the mitochondria depolarized the matrix membrane to inhibit ATP production. However, the opposite effect has also been proposed, namely that an increase in $[Ca^{2+}]_i$ might facilitate ATP production by activating dehydrogenases within the TCA cycle (Cortassa et al., 2003). The net effect of $[Ca^{2+}]_i$ on ATP production is not quantitatively known at present. Therefore, it will be important to include more precise models for glycolysis (Smolen, 1995; Bertram et al., 2004), TCA cycle, and oxidative phosphorylation (Dzbek and Korzeniewski, 2008) in future formulations.

We thank Professor T. Powell for fruitful discussion and for improving the English of this paper.

This work was supported by the Biomedical Cluster Kansai project; a Grant-in-Aid (22590216 to C.Y. Cha and 22390039 to A. Noma) from the Ministry of Education, Culture, Sports, Science and Technology of Japan; and the Ritsumeikan-Global Innovation Research Organization at Ritsumeikan University.

Lawrence G. Palmer served as editor.

Submitted: 7 February 2011
Accepted: 7 June 2011

## REFERENCES

Ämmälä, C., P.O. Berggren, K. Bokvist, and P. Rorsman. 1992. Inhibition of L-type calcium channels by internal GTP [gamma S] in mouse pancreatic beta cells. *Pflugers Arch.* 420:72–77. doi:10.1007/BF00378643

Antunes, C.M., A.P. Salgado, L.M. Rosário, and R.M. Santos. 2000. Differential patterns of glucose-induced electrical activity and intracellular calcium responses in single mouse and rat pancreatic islets. *Diabetes.* 49:2028–2038. doi:10.2337/diabetes.49.12.2028

Arkhammar, P., L. Juntti-Berggren, O. Larsson, M. Welsh, E. Nånberg, A. Sjöholm, M. Köhler, and P.O. Berggren. 1994. Protein kinase C modulates the insulin secretory process by maintaining a proper function of the beta-cell voltage-activated $Ca^{2+}$ channels. *J. Biol. Chem.* 269:2743–2749.

Ashcroft, F.M., and M. Kakei. 1989. ATP-sensitive $K^+$ channels in rat pancreatic beta-cells: modulation by ATP and $Mg^{2+}$ ions. *J. Physiol.* 416:349–367.

Ashcroft, F.M., and P. Rorsman. 1989. Electrophysiology of the pancreatic beta-cell. *Prog. Biophys. Mol. Biol.* 54:87–143. doi:10.1016/0079-6107(89)90013-8

Ashcroft, F.M., D.E. Harrison, and S.J. Ashcroft. 1984. Glucose induces closure of single potassium channels in isolated rat pancreatic beta-cells. *Nature.* 312:446–448. doi:10.1038/312446a0

Atwater, I., B. Ribalet, and E. Rojas. 1979. Mouse pancreatic beta-cells: tetraethylammonium blockage of the potassium permeability increase induced by depolarization. *J. Physiol.* 288:561–574.

Bertram, R., and A. Sherman. 2004. A calcium-based phantom bursting model for pancreatic islets. *Bull. Math. Biol.* 66:1313–1344. doi:10.1016/j.bulm.2003.12.005

Bertram, R., M.J. Butte, T. Kiemel, and A. Sherman. 1995a. Topological and phenomenological classification of bursting oscillations. *Bull. Math. Biol.* 57:413–439.

Bertram, R., P. Smolen, A. Sherman, D. Mears, I. Atwater, F. Martin, and B. Soria. 1995b. A role for calcium release-activated current (CRAC) in cholinergic modulation of electrical activity in pancreatic beta-cells. *Biophys. J.* 68:2323–2332. doi:10.1016/S0006-3495(95)80414-5

Bertram, R., J. Previte, A. Sherman, T.A. Kinard, and L.S. Satin. 2000. The phantom burster model for pancreatic beta-cells. *Biophys. J.* 79:2880–2892. doi:10.1016/S0006-3495(00)76525-8

Bertram, R., L. Satin, M. Zhang, P. Smolen, and A. Sherman. 2004. Calcium and glycolysis mediate multiple bursting modes in pancreatic islets. *Biophys. J.* 87:3074–3087. doi:10.1529/biophysj.104.049262

Bokvist, K., C. Ämmälä, P.O. Berggren, P. Rorsman, and K. Wåhlander. 1991. Alpha 2-adrenoreceptor stimulation does not inhibit L-type calcium channels in mouse pancreatic beta-cells. *Biosci. Rep.* 11:147–157. doi:10.1007/BF01182483

Bozem, M., and J.C. Henquin. 1988. Glucose modulation of spike activity independently from changes in slow waves of membrane potential in mouse B-cells. *Pflugers Arch.* 413:147–152. doi:10.1007/BF00582524

Braun, M., R. Ramracheya, M. Bengtsson, Q. Zhang, J. Karanauskaite, C. Partridge, P.R. Johnson, and P. Rorsman. 2008. Voltage-gated ion channels in human pancreatic beta-cells: electrophysiological characterization and role in insulin secretion. *Diabetes.* 57:1618–1628. doi:10.2337/db07-0991

Brini, M., and E. Carafoli. 2009. Calcium pumps in health and disease. *Physiol. Rev.* 89:1341–1378. doi:10.1152/physrev.00032.2008

Caride, A.J., A.R. Penheiter, A.G. Filoteo, Z. Bajzer, A. Enyedi, and J.T. Penniston. 2001. The plasma membrane calcium pump displays memory of past calcium spikes. Differences between isoforms 2b and 4b. *J. Biol. Chem.* 276:39797–39804. doi:10.1074/jbc.M104380200

Cha, C.Y., Y. Himeno, T. Shimayoshi, A. Amano, and A. Noma. 2009. A novel method to quantify contribution of channels and transporters to membrane potential dynamics. *Biophys. J.* 97:3086–3094. doi:10.1016/j.bpj.2009.08.060

Cha, C.Y., E. Santos, A. Amano, T. Shimayoshi, and A. Noma. 2011. Time-dependent changes in membrane excitability during glucose-induced bursting activity in pancreatic β cells. *J. Gen. Physiol.* 138:39–47.

Chapman, J.B., E.A. Johnson, and J.M. Kootsey. 1983. Electrical and biochemical properties of an enzyme model of the sodium pump. *J. Membr. Biol.* 74:139–153. doi:10.1007/BF01870503

Chay, T.R. 1996. Electrical bursting and luminal calcium oscillation in excitable cell models. *Biol. Cybern.* 75:419–431. doi:10.1007/s004220050307

Chay, T.R. 1997. Effects of extracellular calcium on electrical bursting and intracellular and luminal calcium oscillations in insulin secreting pancreatic beta-cells. *Biophys. J.* 73:1673–1688. doi:10.1016/S0006-3495(97)78199-2

Chay, T.R., and J. Keizer. 1983. Minimal model for membrane oscillations in the pancreatic beta-cell. *Biophys. J.* 42:181–190. doi:10.1016/S0006-3495(83)84384-7

Cheng, H., A. Beck, P. Launay, S.A. Gross, A.J. Stokes, J.P. Kinet, A. Fleig, and R. Penner. 2007. TRPM4 controls insulin secretion in pancreatic beta-cells. *Cell Calcium.* 41:51–61. doi:10.1016/j.ceca.2006.04.032

Chow, R.H., P.E. Lund, S. Löser, U. Panten, and E. Gylfe. 1995. Coincidence of early glucose-induced depolarization with lowering of cytoplasmic $Ca^{2+}$ in mouse pancreatic beta-cells. *J. Physiol.* 485:607–617.

Colsoul, B., A. Schraenen, K. Lemaire, R. Quintens, L. Van Lommel, A. Segal, G. Owsianik, K. Talavera, T. Voets, R.F. Margolskee, et al. 2010. Loss of high-frequency glucose-induced $Ca^{2+}$ oscillations in pancreatic islets correlates with impaired glucose tolerance in Trpm5-/- mice. *Proc. Natl. Acad. Sci. USA.* 107:5208–5213. doi:10.1073/pnas.0913107107

Cook, D.L., and C.N. Hales. 1984. Intracellular ATP directly blocks $K^+$ channels in pancreatic B-cells. *Nature.* 311:271–273. doi:10.1038/311271a0

Cortassa, S., M.A. Aon, E. Marbán, R.L. Winslow, and B. O'Rourke. 2003. An integrated model of cardiac mitochondrial energy metabolism and calcium dynamics. *Biophys. J.* 84:2734–2755. doi:10.1016/S0006-3495(03)75079-6

Dean, P.M., E.K. Matthews, and Y. Sakamoto. 1975. Pancreatic islet cells: effects of monosaccharides, glycolytic intermediates and metabolic inhibitors on membrane potential and electrical activity. *J. Physiol.* 246:459–478.

Diederichs, F. 2006. Mathematical simulation of membrane processes and metabolic fluxes of the pancreatic beta-cell. *Bull. Math. Biol.* 68:1779–1818. doi:10.1007/s11538-005-9053-9

Düfer, M., B. Gier, D. Wolpers, P. Krippeit-Drews, P. Ruth, and G. Drews. 2009. Enhanced glucose tolerance by SK4 channel inhibition in pancreatic beta-cells. *Diabetes.* 58:1835–1843. doi:10.2337/db08-1324

Dunne, M.J., and O.H. Petersen. 1986. Intracellular ADP activates $K^+$ channels that are inhibited by ATP in an insulin-secreting cell line. *FEBS Lett.* 208:59–62. doi:10.1016/0014-5793(86)81532-0

Dzbek, J., and B. Korzeniewski. 2008. Control over the contribution of the mitochondrial membrane potential (DeltaPsi) and proton gradient (DeltapH) to the protonmotive force (Deltap). In silico studies. *J. Biol. Chem.* 283:33232–33239. doi:10.1074/jbc.M802404200

Elwess, N.L., A.G. Filoteo, A. Enyedi, and J.T. Penniston. 1997. Plasma membrane $Ca^{2+}$ pump isoforms 2a and 2b are unusually responsive to calmodulin and $Ca^{2+}$. *J. Biol. Chem.* 272:17981–17986. doi:10.1074/jbc.272.29.17981

Enyedi, A., A.G. Filoteo, G. Gardos, and J.T. Penniston. 1991. Calmodulin-binding domains from isozymes of the plasma membrane $Ca^{2+}$ pump have different regulatory properties. *J. Biol. Chem.* 266:8952–8956.

Fridlyand, L.E., N. Tamarina, and L.H. Philipson. 2003. Modeling of $Ca^{2+}$ flux in pancreatic beta-cells: role of the plasma membrane and intracellular stores. *Am. J. Physiol. Endocrinol. Metab.* 285:E138–E154.

Fridlyand, L.E., L. Ma, and L.H. Philipson. 2005. Adenine nucleotide regulation in pancreatic beta-cells: modeling of ATP/ADP-$Ca^{2+}$ interactions. *Am. J. Physiol. Endocrinol. Metab.* 289:E839–E848. doi:10.1152/ajpendo.00595.2004

Fridlyand, L.E., D.A. Jacobson, A. Kuznetsov, and L.H. Philipson. 2009. A model of action potentials and fast $Ca^{2+}$ dynamics in pancreatic beta-cells. *Biophys. J.* 96:3126–3139. doi:10.1016/j.bpj.2009.01.029

Fridlyand, L.E., N. Tamarina, and L.H. Philipson. 2010. Bursting and calcium oscillations in pancreatic beta-cells: specific pacemakers for specific mechanisms. *Am. J. Physiol. Endocrinol. Metab.* 299:E517–E532. doi:10.1152/ajpendo.00177.2010

Gall, D., J. Gromada, I. Susa, P. Rorsman, A. Herchuelz, and K. Bokvist. 1999. Significance of Na/Ca exchange for $Ca^{2+}$ buffering and electrical activity in mouse pancreatic beta-cells. *Biophys. J.* 76:2018–2028. doi:10.1016/S0006-3495(99)77359-5

Gilon, P., and J.C. Henquin. 1992. Influence of membrane potential changes on cytoplasmic $Ca^{2+}$ concentration in an electrically excitable cell, the insulin-secreting pancreatic B-cell. *J. Biol. Chem.* 267:20713–20720.

Gilon, P., J. Yakel, J. Gromada, Y. Zhu, J.C. Henquin, and P. Rorsman. 1997. G protein-dependent inhibition of L-type $Ca^{2+}$ currents by acetylcholine in mouse pancreatic B-cells. *J. Physiol.* 499:65–76.

Gilon, P., A. Arredouani, P. Gailly, J. Gromada, and J.C. Henquin. 1999. Uptake and release of $Ca^{2+}$ by the endoplasmic reticulum contribute to the oscillations of the cytosolic $Ca^{2+}$ concentration triggered by $Ca^{2+}$ influx in the electrically excitable pancreatic B-cell. *J. Biol. Chem.* 274:20197–20205. doi:10.1074/jbc.274.29.20197

Goforth, P.B., R. Bertram, F.A. Khan, M. Zhang, A. Sherman, and L.S. Satin. 2002. Calcium-activated $K^+$ channels of mouse β-cells are controlled by both store and cytoplasmic $Ca^{2+}$: experimental and theoretical studies. *J. Gen. Physiol.* 120:307–322. doi:10.1085/jgp.20028581

Göpel, S.O., T. Kanno, S. Barg, L. Eliasson, J. Galvanovskis, E. Renström, and P. Rorsman. 1999a. Activation of $Ca^{2+}$-dependent $K^+$ channels contributes to rhythmic firing of action potentials in mouse pancreatic β cells. *J. Gen. Physiol.* 114:759–770. doi:10.1085/jgp.114.6.759

Göpel, S., T. Kanno, S. Barg, J. Galvanovskis, and P. Rorsman. 1999b. Voltage-gated and resting membrane currents recorded from B-cells in intact mouse pancreatic islets. *J. Physiol.* 521:717–728. doi:10.1111/j.1469-7793.1999.00717.x

Grapengiesser, E. 1996. Glucose induces cytoplasmic $Na^+$ oscillations in pancreatic beta-cells. *Biochem. Biophys. Res. Commun.* 226:830–835. doi:10.1006/bbrc.1996.1436

Grapengiesser, E. 1998. Unmasking of a periodic $Na^+$ entry into glucose-stimulated pancreatic beta-cells after partial inhibition of the Na/K pump. *Endocrinology.* 139:3227–3231. doi:10.1210/en.139.7.3227

Hao, L., J.L. Rigaud, and G. Inesi. 1994. $Ca^{2+}/H^+$ countertransport and electrogenicity in proteoliposomes containing erythrocyte plasma membrane Ca-ATPase and exogenous lipids. *J. Biol. Chem.* 269:14268–14275.

Henquin, J.C. 1990. Role of voltage- and $Ca^{2+}$-dependent $K^+$ channels in the control of glucose-induced electrical activity in pancreatic B-cells. *Pflugers Arch.* 416:568–572. doi:10.1007/BF00382691

Henquin, J.C., and H.P. Meissner. 1984a. Effects of theophylline and dibutyryl cyclic adenosine monophosphate on the membrane potential of mouse pancreatic beta-cells. *J. Physiol.* 351:595–612.

Henquin, J.C., and H.P. Meissner. 1984b. Significance of ionic fluxes and changes in membrane potential for stimulus-secretion coupling in pancreatic B-cells. *Experientia.* 40:1043–1052. doi:10.1007/BF01971450

Henquin, J.C., H.P. Meissner, and W. Schmeer. 1982. Cyclic variations of glucose-induced electrical activity in pancreatic B cells. *Pflugers Arch.* 393:322–327. doi:10.1007/BF00581418

Henquin, J.C., M. Nenquin, M.A. Ravier, and A. Szollosi. 2009. Shortcomings of current models of glucose-induced insulin secretion. *Diabetes Obes. Metab.* 11:168–179. doi:10.1111/j.1463-1326.2009.01109.x

Herchuelz, A., A. Kamagate, H. Ximenes, and F. Van Eylen. 2007. Role of Na/Ca exchange and the plasma membrane $Ca^{2+}$-ATPase in beta cell function and death. *Ann. NY Acad. Sci.* 1099:456–467. doi:10.1196/annals.1387.048

Herrington, J., M. Sanchez, D. Wunderler, L. Yan, R.M. Bugianesi, I.E. Dick, S.A. Clark, R.M. Brochu, B.T. Priest, M.G. Kohler, and O.B. McManus. 2005. Biophysical and pharmacological properties of the voltage-gated potassium current of human pancreatic beta-cells. *J. Physiol.* 567:159–175. doi:10.1113/jphysiol.2005.089375

Himeno, Y., F. Toyoda, H. Satoh, A. Amano, C.Y. Cha, H. Matsuura, and A. Noma. 2011. Minor contribution of cytosolic $Ca^{2+}$ transients to the pacemaker rhythm in guinea pig sinoatrial node cells. *Am. J. Physiol. Heart Circ. Physiol.* 300:H251–H261. doi:10.1152/ajpheart.00764.2010

Hiriart, M., and D.R. Matteson. 1988. Na channels and two types of Ca channels in rat pancreatic B cells identified with the reverse hemolytic plaque assay. *J. Gen. Physiol.* 91:617–639. doi:10.1085/jgp.91.5.617

Hirschberg, B., J. Maylie, J.P. Adelman, and N.V. Marrion. 1998. Gating of recombinant small-conductance Ca-activated $K^+$ channels by calcium. *J. Gen. Physiol.* 111:565–581. doi:10.1085/jgp.111.4.565

Hopkins, W.F., S. Fatherazi, B. Peter-Riesch, B.E. Corkey, and D.L. Cook. 1992. Two sites for adenine-nucleotide regulation of ATP-sensitive potassium channels in mouse pancreatic beta-cells and HIT cells. *J. Membr. Biol.* 129:287–295.

Hoth, M., and R. Penner. 1993. Calcium release-activated calcium current in rat mast cells. *J. Physiol.* 465:359–386.

Houamed, K.M., I.R. Sweet, and L.S. Satin. 2010. BK channels mediate a novel ionic mechanism that regulates glucose-dependent electrical activity and insulin secretion in mouse pancreatic β-cells. *J. Physiol.* 588:3511–3523. doi:10.1113/jphysiol.2009.184341

Islam, M.S., O. Larsson, T. Nilsson, and P.O. Berggren. 1995. Effects of caffeine on cytoplasmic free $Ca^{2+}$ concentration in pancreatic beta-cells are mediated by interaction with ATP-sensitive $K^+$ channels and L-type voltage-gated $Ca^{2+}$ channels but not the ryanodine receptor. *Biochem. J.* 306:679–686.

Jacobson, D.A., F. Mendez, M. Thompson, J. Torres, O. Cochet, and L.H. Philipson. 2010. Calcium-activated and voltage-gated potassium channels of the pancreatic islet impart distinct and complementary roles during secretagogue induced electrical responses. *J. Physiol.* 588:3525–3537. doi:10.1113/jphysiol.2010.190207

Kanno, T., P. Rorsman, and S.O. Göpel. 2002. Glucose-dependent regulation of rhythmic action potential firing in pancreatic beta-cells by $K_{ATP}$-channel modulation. *J. Physiol.* 545:501–507. doi:10.1113/jphysiol.2002.031344

Keizer, J., and G. Magnus. 1989. ATP-sensitive potassium channel and bursting in the pancreatic beta cell. A theoretical study. *Biophys. J.* 56:229–242. doi:10.1016/S0006-3495(89)82669-4

Kelly, R.P., R. Sutton, and F.M. Ashcroft. 1991. Voltage-activated calcium and potassium currents in human pancreatic beta-cells. *J. Physiol.* 443:175–192.

Kinard, T.A., G. de Vries, A. Sherman, and L.S. Satin. 1999. Modulation of the bursting properties of single mouse pancreatic beta-cells by artificial conductances. *Biophys. J.* 76:1423–1435. doi:10.1016/S0006-3495(99)77303-0

Kukuljan, M., A.A. Goncalves, and I. Atwater. 1991. Charybdotoxin-sensitive $K(_{Ca})$ channel is not involved in glucose-induced electrical activity in pancreatic beta-cells. *J. Membr. Biol.* 119:187–195. doi:10.1007/BF01871418

Larsson, O., H. Kindmark, R. Brandstrom, B. Fredholm, and P.O. Berggren. 1996. Oscillations in $K_{ATP}$ channel activity promote oscillations in cytoplasmic free $Ca^{2+}$ concentration in the pancreatic beta cell. *Proc. Natl. Acad. Sci. USA.* 93:5161–5165. doi:10.1073/pnas.93.10.5161

Leech, C.A., and J.F. Habener. 1998. A role for $Ca^{2+}$-sensitive nonselective cation channels in regulating the membrane potential of pancreatic beta-cells. *Diabetes.* 47:1066–1073. doi:10.2337/diabetes.47.7.1066

Lytton, J., M. Westlin, S.E. Burk, G.E. Shull, and D.H. MacLennan. 1992. Functional comparisons between isoforms of the sarcoplasmic or endoplasmic reticulum family of calcium pumps. *J. Biol. Chem.* 267:14483–14489.

MacDonald, P.E., A.M. Salapatek, and M.B. Wheeler. 2003. Temperature and redox state dependence of native Kv2.1 currents in rat pancreatic beta-cells. *J. Physiol.* 546:647–653. doi:10.1113/jphysiol.2002.035709

Magnus, G., and J. Keizer. 1998. Model of beta-cell mitochondrial calcium handling and electrical activity. I. Cytoplasmic variables. *Am. J. Physiol.* 274:C1158–C1173.

Marigo, V., K. Courville, W.H. Hsu, J.M. Feng, and H. Cheng. 2009. TRPM4 impacts on $Ca^{2+}$ signals during agonist-induced insulin secretion in pancreatic beta-cells. *Mol. Cell. Endocrinol.* 299:194–203. doi:10.1016/j.mce.2008.11.011

Mears, D., N.F. Sheppard Jr., I. Atwater, E. Rojas, R. Bertram, and A. Sherman. 1997. Evidence that calcium release-activated current mediates the biphasic electrical activity of mouse pancreatic beta-cells. *J. Membr. Biol.* 155:47–59. doi:10.1007/s002329900157

Meissner, H.P., and H. Schmelz. 1974. Membrane potential of beta-cells in pancreatic islets. *Pflugers Arch.* 351:195–206. doi:10.1007/BF00586918

Merrins, M.J., B. Fendler, M. Zhang, A. Sherman, R. Bertram, and L.S. Satin. 2010. Metabolic oscillations in pancreatic islets depend on the intracellular $Ca^{2+}$ level but not $Ca^{2+}$ oscillations. *Biophys. J.* 99:76–84. doi:10.1016/j.bpj.2010.04.012

Meyer-Hermann, M.E. 2007. The electrophysiology of the beta-cell based on single transmembrane protein characteristics. *Biophys. J.* 93:2952–2968. doi:10.1529/biophysj.107.106096

Misler, S., L.C. Falke, K. Gillis, and M.L. McDaniel. 1986. A metabolite-regulated potassium channel in rat pancreatic B cells. *Proc. Natl. Acad. Sci. USA.* 83:7119–7123. doi:10.1073/pnas.83.18.7119

Miura, Y., J.C. Henquin, and P. Gilon. 1997. Emptying of intracellular $Ca^{2+}$ stores stimulates $Ca^{2+}$ entry in mouse pancreatic beta-cells by both direct and indirect mechanisms. *J. Physiol.* 503:387–398. doi:10.1111/j.1469-7793.1997.387bh.x

Miwa, Y., and Y. Imai. 1999. Simulation of spike-burst generation and $Ca^{2+}$ oscillation in pancreatic beta-cells. *Jpn. J. Physiol.* 49:353–364. doi:10.2170/jjphysiol.49.353

Oka, C., C.Y. Cha, and A. Noma. 2010. Characterization of the cardiac $Na^+/K^+$ pump by development of a comprehensive and mechanistic model. *J. Theor. Biol.* 265:68–77. doi:10.1016/j.jtbi.2010.04.028

Owada, S., O. Larsson, P. Arkhammar, A.I. Katz, A.V. Chibalin, P.O. Berggren, and A.M. Bertorello. 1999. Glucose decreases $Na^+,K^+$-ATPase activity in pancreatic beta-cells. An effect mediated via $Ca^{2+}$-independent phospholipase A2 and protein kinase C-dependent phosphorylation of the alpha-subunit. *J. Biol. Chem.* 274:2000–2008. doi:10.1074/jbc.274.4.2000

Plant, T.D. 1988. Properties and calcium-dependent inactivation of calcium currents in cultured mouse pancreatic B-cells. *J. Physiol.* 404:731–747.

Prakriya, M., and R.S. Lewis. 2002. Separation and characterization of currents through store-operated CRAC channels and $Mg^{2+}$-inhibited cation (MIC) channels. *J. Gen. Physiol.* 119:487–507. doi:10.1085/jgp.20028551

Ribalet, B., and P.M. Beigelman. 1980. Calcium action potentials and potassium permeability activation in pancreatic beta-cells. *Am. J. Physiol.* 239:C124–C133.

Roe, M.W., L.H. Philipson, C.J. Frangakis, A. Kuznetsov, R.J. Mertz, M.E. Lancaster, B. Spencer, J.F. Worley III, and I.D. Dukes. 1994.

Defective glucose-dependent endoplasmic reticulum $Ca^{2+}$ sequestration in diabetic mouse islets of Langerhans. *J. Biol. Chem.* 269:18279–18282.

Rorsman, P., and G. Trube. 1985. Glucose dependent $K^+$-channels in pancreatic beta-cells are regulated by intracellular ATP. *Pflugers Arch.* 405:305–309. doi:10.1007/BF00595682

Rorsman, P., and G. Trube. 1986. Calcium and delayed potassium currents in mouse pancreatic beta-cells under voltage-clamp conditions. *J. Physiol.* 374:531–550.

Rorsman, P., H. Abrahamsson, E. Gylfe, and B. Hellman. 1984. Dual effects of glucose on the cytosolic $Ca^{2+}$ activity of mouse pancreatic beta-cells. *FEBS Lett.* 170:196–200. doi:10.1016/0014-5793(84)81398-8

Rorsman, P., P. Arkhammar, and P.O. Berggren. 1986. Voltage-activated $Na^+$ currents and their suppression by phorbol ester in clonal insulin-producing RINm5F cells. *Am. J. Physiol.* 251:C912–C919.

Rorsman, P., C. Ämmälä, P.O. Berggren, K. Bokvist, and O. Larsson. 1992. Cytoplasmic calcium transients due to single action potentials and voltage-clamp depolarizations in mouse pancreatic B-cells. *EMBO J.* 11:2877–2884.

Santos, R.M., and E. Rojas. 1989. Muscarinic receptor modulation of glucose-induced electrical activity in mouse pancreatic B-cells. *FEBS Lett.* 249:411–417. doi:10.1016/0014-5793(89)80669-6

Santos, R.M., L.M. Rosario, A. Nadal, J. Garcia-Sancho, B. Soria, and M. Valdeolmillos. 1991. Widespread synchronous $[Ca^{2+}]_i$ oscillations due to bursting electrical activity in single pancreatic islets. *Pflugers Arch.* 418:417–422. doi:10.1007/BF00550880

Satin, L.S., and D.L. Cook. 1989. Calcium current inactivation in insulin-secreting cells is mediated by calcium influx and membrane depolarization. *Pflugers Arch.* 414:1–10. doi:10.1007/BF00585619

Satin, L.S., W.F. Hopkins, S. Fatherazi, and D.L. Cook. 1989. Expression of a rapid, low-voltage threshold K current in insulin-secreting cells is dependent on intracellular calcium buffering. *J. Membr. Biol.* 112:213–222. doi:10.1007/BF01870952

Schulla, V., E. Renström, R. Feil, S. Feil, I. Franklin, A. Gjinovci, X.J. Jing, D. Laux, I. Lundquist, M.A. Magnuson, et al. 2003. Impaired insulin secretion and glucose tolerance in beta cell-selective $Ca_v1.2$ $Ca^{2+}$ channel null mice. *EMBO J.* 22:3844–3854. doi:10.1093/emboj/cdg389

Sherman, A., J. Rinzel, and J. Keizer. 1988. Emergence of organized bursting in clusters of pancreatic beta-cells by channel sharing. *Biophys. J.* 54:411–425. doi:10.1016/S0006-3495(88)82975-8

Sherman, A., J. Keizer, and J. Rinzel. 1990. Domain model for $Ca^{2+}$-inactivation of $Ca^{2+}$ channels at low channel density. *Biophys. J.* 58:985–995. doi:10.1016/S0006-3495(90)82443-7

Smith, P.A., P. Rorsman, and F.M. Ashcroft. 1989. Modulation of dihydropyridine-sensitive $Ca^{2+}$ channels by glucose metabolism in mouse pancreatic beta-cells. *Nature.* 342:550–553. doi:10.1038/342550a0

Smith, P.A., F.M. Ashcroft, and P. Rorsman. 1990a. Simultaneous recordings of glucose dependent electrical activity and ATP-regulated $K^+$-currents in isolated mouse pancreatic beta-cells. *FEBS Lett.* 261:187–190. doi:10.1016/0014-5793(90)80667-8

Smith, P.A., K. Bokvist, P. Arkhammar, P.O. Berggren, and P. Rorsman. 1990b. Delayed rectifying and calcium-activated $K^+$ channels and their significance for action potential repolarization in mouse pancreatic β-cells. *J. Gen. Physiol.* 95:1041–1059. doi:10.1085/jgp.95.6.1041

Smolen, P. 1995. A model for glycolytic oscillations based on skeletal muscle phosphofructokinase kinetics. *J. Theor. Biol.* 174:137–148. doi:10.1006/jtbi.1995.0087

Smolen, P., and J. Keizer. 1992. Slow voltage inactivation of $Ca^{2+}$ currents and bursting mechanisms for the mouse pancreatic beta-cell. *J. Membr. Biol.* 127:9–19.

Sturgess, N.C., C.N. Hales, and M.L. Ashford. 1987. Calcium and ATP regulate the activity of a non-selective cation channel in a rat insulinoma cell line. *Pflugers Arch.* 409:607–615. doi:10.1007/BF00584661

Takeuchi, A., S. Tatsumi, N. Sarai, K. Terashima, S. Matsuoka, and A. Noma. 2006. Ionic mechanisms of cardiac cell swelling induced by blocking $Na^+/K^+$ pump as revealed by experiments and simulation. *J. Gen. Physiol.* 128:495–507. doi:10.1085/jgp.200609646

Tamarina, N.A., Y. Wang, L. Mariotto, A. Kuznetsov, C. Bond, J. Adelman, and L.H. Philipson. 2003. Small-conductance calcium-activated $K^+$ channels are expressed in pancreatic islets and regulate glucose responses. *Diabetes.* 52:2000–2006. doi:10.2337/diabetes.52.8.2000

Tengholm, A., B. Hellman, and E. Gylfe. 2001. The endoplasmic reticulum is a glucose-modulated high-affinity sink for $Ca^{2+}$ in mouse pancreatic beta-cells. *J. Physiol.* 530:533–540. doi:10.1111/j.1469-7793.2001.0533k.x

Tse, F.W., A. Tse, and B. Hille. 1994. Cyclic $Ca^{2+}$ changes in intracellular stores of gonadotropes during gonadotropin-releasing hormone-stimulated $Ca^{2+}$ oscillations. *Proc. Natl. Acad. Sci. USA.* 91:9750–9754. doi:10.1073/pnas.91.21.9750

Váradi, A., E. Molnár, and S.J. Ashcroft. 1995. Characterisation of endoplasmic reticulum and plasma membrane $Ca^{2+}$-ATPases in pancreatic beta-cells and in islets of Langerhans. *Biochim. Biophys. Acta.* 1236:119–127. doi:10.1016/0005-2736(95)00103-A

Váradi, A., E. Molnár, C.G. Ostenson, and S.J. Ashcroft. 1996. Isoforms of endoplasmic reticulum $Ca^{2+}$-ATPase are differentially expressed in normal and diabetic islets of Langerhans. *Biochem. J.* 319:521–527.

Velasco, J.M., and O.H. Petersen. 1987. Voltage-activation of high-conductance $K^+$ channel in the insulin-secreting cell line RINm5F is dependent on local extracellular Ca2+ concentration. *Biochim. Biophys. Acta.* 896:305–310. doi:10.1016/0005-2736(87)90191-X

Vignali, S., V. Leiss, R. Karl, F. Hofmann, and A. Welling. 2006. Characterization of voltage-dependent sodium and calcium channels in mouse pancreatic A- and B-cells. *J. Physiol.* 572:691–706.

Worley, J.F., III, M.S. McIntyre, B. Spencer, and I.D. Dukes. 1994a. Depletion of intracellular $Ca^{2+}$ stores activates a maitotoxin-sensitive nonselective cationic current in beta-cells. *J. Biol. Chem.* 269:32055–32058.

Worley, J.F., III, M.S. McIntyre, B. Spencer, R.J. Mertz, M.W. Roe, and I.D. Dukes. 1994b. Endoplasmic reticulum calcium store regulates membrane potential in mouse islet beta-cells. *J. Biol. Chem.* 269:14359–14362.

Zhang, M., P. Goforth, R. Bertram, A. Sherman, and L. Satin. 2003. The $Ca^{2+}$ dynamics of isolated mouse beta-cells and islets: implications for mathematical models. *Biophys. J.* 84:2852–2870. doi:10.1016/S0006-3495(03)70014-9

Zhang, M., K. Houamed, S. Kupershmidt, D. Roden, and L.S. Satin. 2005. Pharmacological properties and functional role of $K_{slow}$ current in mouse pancreatic β-cells: SK channels contribute to $K_{slow}$ tail current and modulate insulin secretion. *J. Gen. Physiol.* 126:353–363. doi:10.1085/jgp.200509312

# Utility of indices using C-peptide levels for indication of insulin therapy to achieve good glycemic control in Japanese patients with type 2 diabetes

Shogo Funakoshi[1], Shimpei Fujimoto[1]*, Akihiro Hamasaki[1], Hideya Fujiwara[1], Yoshihito Fujita[1], Kaori Ikeda[1], Shiho Takahara[1], Kazuaki Nagashima[1], Masaya Hosokawa[1], Yutaka Seino[2], Nobuya Inagaki[1]

## ABSTRACT

**Aims/Introduction:** Type 2 diabetes is progressive in that therapy must be altered over time, which is partly as a result of the progressive loss of pancreatic β-cell function. To elucidate the relationship between residual endogenous insulin secretion and the necessity of insulin therapy to achieve good glycemic control, indices using serum C-peptide immunoreactivity (CPR) were analyzed in patients with type 2 diabetes.

**Materials and Methods:** The data of 201 Japanese patients with type 2 diabetes who achieved the target of glycemic control during admission were analyzed retrospectively. Indices using CPR including fasting CPR (FCPR), CPR 6 min after intravenous injection of glucagon (CPR-6 min), increment of CPR (ΔCPR), secretory unit of islet in transplantation index (SUIT) and C-peptide index (CPI) were compared between the group requiring insulin (insulin group) and the group not requiring insulin (non-insulin group). A receiver–operator characteristic (ROC) curve was made, and optimal cut-off point and likelihood ratio were determined for each index.

**Results:** All indices of CPR were lower in the insulin group compared with those in the non-insulin group. Likelihood ratios at the optimal point of FCPR, CPR-6 min, ΔCPR, SUIT, and CPI were 2.0, 2.1, 1.6, 2.3 and 2.8, respectively. Optimal cut-off point of CPI was 1.1 ng/mg. Sensitivity and specificity at optimal point of CPI were 61 and 78%, respectively.

**Conclusions:** The advantage of CPI of the indices of CPR to select insulin therapy to achieve good glycemic control was shown, but limitations of the predictive abilities of the indices using CPR should be taken into account. (J Diabetes Invest, doi: 10.1111/j.2040-1124.2010.00096.x, 2011)

**KEY WORDS: C-peptide, Insulin therapy, Glycemic control**

## INTRODUCTION

Type 2 diabetes is a heterogeneous disease characterized by insulin resistance and defective insulin secretion[1], and is progressive in that therapy must be altered over time. Initially on diagnosis, diet and exercise are generally adequate to achieve good glycemic control; oral hypoglycemic agents (OHA) are required later, when patients cannot achieve control with diet and exercise alone. Daily insulin injection is indicated when patients are unable to achieve control with a combination of oral agents, diet and exercise[2,3]. Insulin therapy is required in these patients not for survival, as is found in type 1 diabetes, but for good glycemic control[4]. This requirement is, at least in part, as a result of the progressive loss of pancreatic β-cell function. The results of the United Kingdom Progressive Diabetes Study (UKPDS) shows that pancreatic β-cell function (%β), assessed by Homeostasis Model Assessment (HOMA) in patients allocated to diet or OHA, decreased approximately 25% in 5 years[5]. A decline in endogenous insulin secretion over more than several decades of diabetes was observed in a cross-sectional study[6].

Determination of fasting serum C-peptide level and stimulated serum C-peptide level by intravenous glucagon is used widely to assess endogenous insulin secretory reserves[7–10]. There are several reports regarding the correlation between levels of residual endogenous insulin secretion and the choice of insulin therapy to achieve glycemic control[11–14]. However, in these studies, because the glycemic goal was not described clearly or was inappropriate, patients with insufficient glycemic control by the selected mode of therapy were sometimes included.

[1]Department of Diabetes and Clinical Nutrition, Graduate School of Medicine, Kyoto University, Kyoto, and [2]Kansai Electric Power Hospital, Osaka, Japan
*Corresponding author. Shimpei Fujimoto Tel.: +81-75-751-3560
Fax: +81-75-751-4244 E-mail address: fujimoto@metab.kuhp.kyoto-u.ac.jp
Received 9 September 2010; revised 12 November 2010; accepted 24 November 2010

In the present study, to evaluate the clinical significance of measures of serum C-peptide in achieving good glycemic control, we retrospectively analyzed the use of indices of endogenous insulin secretion in type 2 diabetes patients admitted to our hospital. Using data of patients who achieved the target of glycemic control during the period of admission, the patients were divided into two groups: one that achieved good control without the use of insulin (non-insulin group) and the other that required the use of insulin (insulin group), and the indices using serum C-peptide were compared between them. Optimal values and the utility of indices using serum C-peptide to select insulin therapy to achieve good glycemic control were analyzed.

## MATERIALS AND METHODS

### Subjects

A total of 746 Japanese patients with type 2 diabetes admitted between 2003 and 2009 to Kyoto University Hospital for poor glycemic control were enrolled in the present study. Type 2 diabetes mellitus was diagnosed based on the criteria of the American Diabetes Association (ADA)[15]. As indicated in Figure S1, 76 patients including those with pancreatic disease and liver disease, those taking diabetogenic medication and pregnant women were excluded. A total of 40 patients with incomplete clinical examinations also were excluded, and 66 patients with serum creatinine ≥1.3 mg/dL were excluded, as serum C-peptide immunoreactivity (CPR) is elevated by decreased renal function[16]. The data of 90 patients taking oral hypoglycemic agents (OHA) plus insulin at discharge were excluded. Good control was defined as mean preprandial capillary plasma glucose level <130 mg/dL, according to the glycemic control recommendation of ADA[17]. The 474 patients were divided into two groups: 201 patients who achieved good glycemic control (achieved group) and 273 patients who did not (non-achieved group). As shown in Figure S2, of the 201 patients in the achieved group, 47, 107, 38 and nine patients were treated with diet alone, OHA, insulin and insulin plus OHA at admission, respectively. At discharge, 24, 95 and 82 patients were treated with diet alone, OHA and insulin, respectively. Patients treated with diet alone and OHA at discharge comprised the non-insulin group; patients treated with insulin at discharge comprised the insulin group. A total of 166 patients of the 474 patients in the achieved or non-achieved group at discharge who could be confirmed within 6 months after discharge to achieve <7.4% in $HbA_{1c}$, which excludes 'not good' and 'poor' for assessment of glycemic control in the treatment guide for diabetes of the Japan Diabetes Society (JDS guide)[18], were re-analyzed to determine the cut-off point for C-peptide index (CPI) for longer duration of glycemic control. Of the 201 patients in the achieved group at discharge, 85 were excluded as a result of readmission or alteration to the mode of therapy, or were not followed as outpatients due to a change of hospital. Of the remaining 116 patients, 90 showed <7.4% $HbA_{1c}$ within 6 months after discharge. Of the 273 patients in the non-achieved group at discharge, 137 were excluded as a result of readmission or alteration to the mode of therapy, or were not followed as outpatients due to a change of hospital. In the remaining 136 patients, 76 achieved <7.4% $HbA_{1c}$ within 6 months after discharge. In these 166 patients, analysis of optimal values and the utility of CPI during admission was carried out.

### Methods

On the first day in hospital, medical history, physical examination and laboratory evaluation including glycosylated hemoglobin were carried out. $HbA_{1c}$ was measured using HPLC (HA-8180; Arcray, Kyoto, Japan). The $HbA_{1c}$ (%) value was estimated as an National Glycohemoglobin Standardization Program equivalent (%) calculated by the formula: $HbA_{1c}$ (%) = $HbA_{1c}$ (JDS) (%) + 0.4%, considering the relational expression of $HbA_{1c}$ (JDS) (%) measured by the previous Japanese standard substance and measurement methods and $HbA_{1c}$ (National Glycohemoglobin Standardization Program)[19]. β-cell function was evaluated within 1 week after overnight fast by glucagon test measuring CPR before (fasting CPR [FCPR]) and 6 min after i.v. injection of 1 mg glucagon (CPR-6 min)[7], as this test is valid in patients taking insulin therapy. Increment of CPR (ΔCPR) was obtained by subtracting FCPR from CPR-6 min. SUIT index (SUIT) (%) was calculated by the formula: 1500 × FCPR (ng/mL)/(fasting plasma glucose [FPG; mg/dL] − 61.7)[20]. CPI (ng/mg) was calculated by the formula: 100 × FCPR (ng/mL)/FPG (mg/dL). Serum CPR was measured by immunoenzymometric assay (EIA; ST AIA-PACK C-Peptide, Toso corporation, Tokyo, Japan). In patients taking OHA, medication was stopped for the glucagon test, but was maintained until 1 day before to prevent hyperglycemia during the test[6]. Fasting plasma glucose was measured by the glucose oxidase method when the glucagon test was carried out. Patients were treated according to the JDS guide[18]. Treatment policy including diet therapy, exercise therapy, pharmacotherapy and education for each patient was determined by Japanese Board Certified Diabetologists certified by the Japan Diabetes Society. Patients took medical nutritional therapy (25–30 kcal/kg of standard bodyweight/day consisting of 58% carbohydrate, 18% protein and 24% fat energy intake percentages) with counseling by a registered dietitian. Preprandial capillary plasma glucose levels were monitored three t.i.d. during hospitalization. The study protocol was approved by the ethics committee of Kyoto University.

### Statistical analysis

Statistical analysis was carried out with the Stat View 5.0 system (SAS institute, Cary, NC, USA). Data are presented as mean ± SE unless otherwise stated. Clinical parameters among the two groups were compared by Mann–Whitney *U*-test. *P*-values <0.01 were considered statistically significant. Histograms and receiver–operator characteristic (ROC) curve were made for FCPR, CPR-6 min, ΔCPR, SUIT and CPI respectively, and sensitivity, specificity, cut-off values, area under the ROC curve (AUC) and the likelihood ratio were calculated.

 

## RESULTS

Clinical profiles of patients with mean preprandial capillary plasma glucose levels at discharge of <130 mg/dL (achieved group) and ≥130 mg/dL (non-achieved group), respectively, are shown in Table 1. Patients of the non-achieved group were older, had lower body mass index at admission, higher mean preprandial capillary plasma glucose level both at admission and at discharge, longer years from diagnosis and lower endogenous insulin secretion indices than those of the achieved group. The clinical stages of diabetic nephropathy and retinopathy were more progressed in the non-achieved group than those in the achieved group. The relationships between indices using serum C-peptide and selected modes of therapy at discharge were analyzed based on the data of the achieved group.

The clinical profiles of patients not requiring insulin for good glycemic control (non-insulin group) and those requiring insulin (insulin group) are shown in Table 2. The patients of the insulin group were older, has lower body mass index, higher $HbA_{1c}$ at admission, higher mean preprandial capillary plasma glucose level at admission, longer years from diagnosis and lower endogenous insulin secretion indices compared with those of the non-insulin group. As shown in Figure S2, the mode of therapy in 41 patients was altered from diet alone or OHA to insulin during admission. The average number of hospital days before altering the therapeutic mode of these patients was 3.1 ± 3.4 (mean ± SD). The reasons for the change to insulin therapy were the necessity of tight glycemic control before operation in five patients, marked hyperglycemia (a fasting plasma glucose level of 250 mg/dL or above, or a causal plasma glucose of 350 mg/dL or above)[21] or both the presence of hyperglycemia and ketosis in 11 patients, and persistent hyperglycemia with OHA in 25 patients. $HbA_{1c}$ at admission of these patients was 10.2 ± 2.2% (mean ± SD). In five patients, the mode of therapy was altered from insulin to OHA. The average number of hospital days before this change was 7.6 ± 4.3 (mean ± SD); the reason was improved glycemic control despite a decrease in the required dosage of insulin. $HbA_{1c}$ at admission of these patients was 10.1 ± 4.4% (mean ± SD). Another patient treated with OHA plus insulin at admission was changed to OHA alone after nine hospital days because of improved glycemic control. Of the 113 patients with therapy of diet alone or OHA both at admission and at discharge, 19 transiently used insulin during the period of admission.

The category of OHA at discharge is shown in Table S1a. In 95 patients treated with OHA, 60 and 29 patients were prescribed sulfonylurea alone or in combination, and biguanide alone or in combination, respectively. In the insulin group, 50 of 86 patients were given premixed insulin b.i.d. at discharge. As shown in Table S1b, the prescribed daily dosages of gliclazide, glimepiride and metformin required were <80, 4 and 750 mg,

**Table 1** | Clinical profiles of patients who achieved good glycemic control

| | Achieved | Non-achieved | *P* |
|---|---|---|---|
| No. subjects | 201 | 273 | |
| Duration of hospitalization (days) | 22.0 ± 0.7 | 23.6 ± 0.7 | 0.1115 |
| Age (years) | 60.2 ± 0.9 | 64.5 ± 0.7* | 0.0002 |
| Male/female | 127/74 | 159/114 | |
| Systolic blood pressure (mmHg) | 124.5 ± 1.0 | 126.9 ± 1.1 | 0.1076 |
| Diastolic blood pressure (mmHg) | 74.6 ± 0.7 | 73.6 ± 0.6 | 0.2653 |
| BMI ($kg/m^2$) | 25.2 ± 0.3 | 23.8 ± 0.3* | 0.0005 |
| $HbA_{1c}$ at admission (%) | 9.5 ± 0.1 | 9.8 ± 0.1 | 0.0776 |
| PG at admission (mg/dL) | 181.1 ± 4.7 | 209.5 ± 3.9* | <0.0001 |
| PG at discharge (mg/dL) | 112.2 ± 0.9 | 163.2 ± 1.9* | <0.0001 |
| Years from diagnosis | 9.1 ± 0.6 | 13.5 ± 0.6* | <0.0001 |
| FCPR (ng/mL) | 1.87 ± 0.06 | 1.65 ± 0.05* | 0.0054 |
| CPR-6 min (ng/mL) | 3.99 ± 0.14 | 3.41 ± 0.10* | 0.0006 |
| ΔCPR (ng/mL) | 2.12 ± 0.09 | 1.76 ± 0.07* | 0.0011 |
| SUIT (%) | 40.6 ± 1.9 | 32.4 ± 2.0* | 0.0043 |
| CPI (ng/mg) | 1.34 ± 0.05 | 1.09 ± 0.04* | <0.0001 |
| Clinical stage of nephropathy (normal/microalbuminuria/macroalbuminuria) | 129/56/16 (64/28/8) | 133/80/60 (49/29/22) | |
| Clinical stage of retinopathy (NDR/mild NPDR/moderate NPDR/severe NPDR/PDR) | 141/25/26/4/5 (71/12/13/2/2) | 112/53/45/22/41 (41/20/16/8/15) | |

Data are presented as mean ± SE. *$P$ < 0.01 versus achieved. Achieved group: mean preprandial capillary plasma glucose levels at discharge <130 mg/dL compared with those who did not achieve good glycemic control (non-achieved group ≥130 mg/dL). BMI, body mass index; CPI, C-peptide index; ΔCPR, increment of C-peptide immunoreactivity; CPR-6 min, C-peptide immunoreactivity 6 min after intravenous injection of glucagon; FCPR, fasting C-peptide immunoreactivity; NDR, no diabetic retinopathy; NPDR, non-proliferative diabetic retinopathy; PDR, proliferative diabetic retinopathy; PG, mean preprandial capillary plasma glucose level; SUIT, secretory unit of islet in transplantation index. Numbers in parentheses indicate percentages.

**Table 2** | Clinical profiles of patients who achieved good glycemic control without requiring the use of insulin and those requiring insulin to achieve good glycemic control

| | Non-insulin | Insulin | *P* |
|---|---|---|---|
| No. subjects | 119 | 82 | |
| Male/female | 82/37 | 45/37 | |
| Age (years) | 58.4 ± 1.1 | 62.9 ± 1.3* | 0.0099 |
| Systolic blood pressure (mmHg) | 124.4 ± 1.4 | 126.4 ± 1.7 | 0.3598 |
| Diastolic blood pressure (mmHg) | 77.3 ± 1.0 | 73.3 ± 1.3 | 0.0135 |
| BMI (kg/m$^2$) | 26.0 ± 0.4 | 24.0 ± 0.4* | 0.0019 |
| $HbA_{1c}$ at admission (%) | 9.2 ± 0.2 | 10.0 ± 0.2* | 0.0050 |
| PG at admission (mg/dL) | 163.2 ± 5.0 | 206.9 ± 8.0* | <0.0001 |
| PG at discharge (mg/dL) | 110.9 ± 1.2 | 114.2 ± 1.3 | 0.0602 |
| Years from diagnosis | 7.8 ± 0.6 | 10.9 ± 1.0* | 0.0052 |
| FCPR (ng/mL) | 2.06 ± 0.07 | 1.61 ± 0.09* | 0.0001 |
| CPR-6 min (ng/mL) | 4.48 ± 0.18 | 3.29 ± 0.19* | <0.0001 |
| ΔCPR (ng/mL) | 2.43 ± 0.12 | 1.68 ± 0.12* | <0.0001 |
| SUIT (%) | 47.2 ± 2.5 | 31.1 ± 2.7* | <0.0001 |
| CPI (ng/mg) | 1.57 ± 0.07 | 1.06 ± 0.06* | <0.0001 |

Data are presented as mean ± SE. *$P$ < 0.01 versus non-insulin. Good glycemic control: mean preprandial capillary plasma glucose levels at discharge <130 mg/dL.
BMI, body mass index; CPI, C-peptide index; ΔCPR, increment of C-peptide immunoreactivity; CPR-6 min, C-peptide immunoreactivity 6 min after intravenous injection of glucagon; FCPR, fasting C-peptide immunoreactivity; PG, mean preprandial capillary plasma glucose level; SUIT, secretory unit of islet in transplantation index.

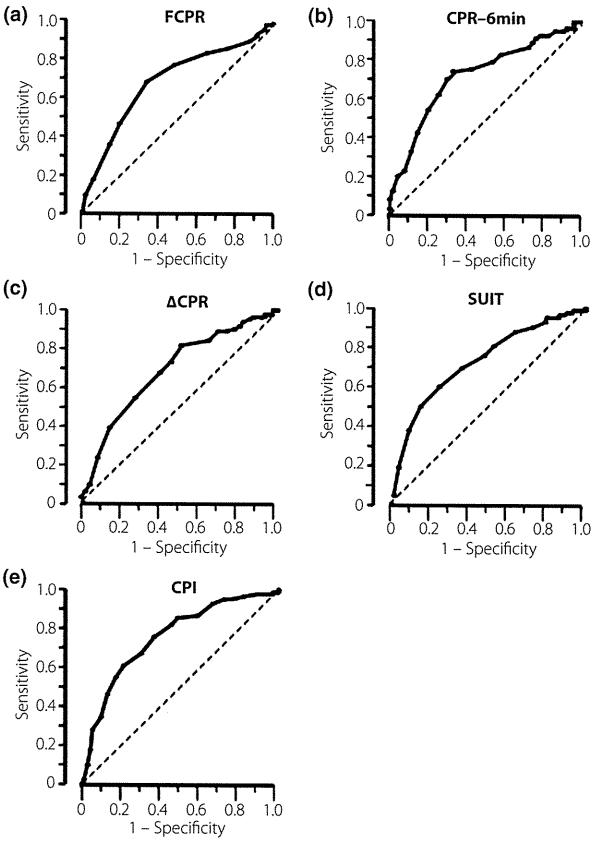


**Figure 1** | Receiver–operator characteristic curves of (a) fasting C-peptide immunoreactivity (FCPR), (b) CPR 6 min after intravenous injection of glucagon (CPR-6 min), (c) increment of CPR (ΔCPR), (d) secretory unit of islet in transplantation index (SUIT) and (e) C-peptide index (CPI) of patients with mean preprandial capillary plasma glucose levels of <130 mg/dL at discharge.

respectively in almost all (more than 95%) patients. Daily insulin dosage was 22.0 ± 11.1 U (mean ± SD) in the insulin group.

In Figure S3, peak relative frequency of indices using CPR of patients with mean preprandial capillary plasma glucose levels of <130 mg/dL at discharge in the insulin group and the non-insulin group, respectively, is shown (FCPR: 1.50–1.75, 2.00–2.25 ng/mL; CPR-6 min: 2.75–3.00, 4.00–4.25 ng/mL; ΔCPR: 1.25–1.50, 1.25–1.50 plus 2.25–2.50 ng/mL; SUIT: 15–20, 25–30 plus 35–40 plus 45–50%; and CPI: 0.8–0.9, 1.5–1.6 ng/mg). According to ROC curves of indices using CPR shown in Figure 1, AUC, cut-off values and values at optimal cut-off points including sensitivity, specificity and the likelihood ratio were determined and shown in Table 3. CPI is the most relevant of these indices for selecting insulin therapy to achieve good glycemic control, because the likelihood ratio and AUC of CPI is greatest.

The ROC curve of CPI of patients who achieved <7.4% $HbA_{1c}$ within 6 months after discharge is shown in Figure 2. According to ROC curves of CPI in Figure 2, the AUC (0.75), cut-off values (optimal: 1.2; 90% specificity 0.8; 90% sensitivity 1.7 ng/mg), and values at optimal cut-off points including sensitivity (73%), specificity (71%) and the likelihood ratio (2.5) were determined.

## DISCUSSION

Medical nutritional therapy (MNT) improves glycemic control in patients with type 2 diabetes regardless of their modes of therapy including diet alone, OHA and insulin[22–24]. Diet therapy is the basis and starting point of treatment of all patients with diabetes[25], and failure of diet therapy alone might predict the inability to attain optimal glycemic control by any of these modes of therapy. To precisely analyze the relationship between endogenous insulin secretion and the appropriate mode of therapy for achieving good glycemic control, we used data of hospitalized patients under optimal therapy including proper MNT. Thus, our results are more likely to be valid in patients with appropriate care behaviors. Although inappropriate care behavior is an obstacle to achieving good glycemic control over a longer duration, our results suggest a basis for beginning insulin therapy in patients who do not achieve good glycemic control with diet alone or OHA despite the practice of appropriate care behavior.

**Table 3** | Analysis of indices using serum C-peptide of patients with mean preprandial capillary plasma glucose levels of <130 mg/dL at discharge

| | FCPR | CPR-6 min | ΔCPR | SUIT | CPI |
|---|---|---|---|---|---|
| AUC | 0.69 | 0.71 | 0.69 | 0.72 | 0.75 |
| Cut-off values | (ng/mL) | (ng/mL) | (ng/mL) | (%) | (ng/mg) |
| Optimal | 1.75 | 3.75 | 2.25 | 30 | 1.1 |
| 90% Specificity | 1.00 | 2.25 | 1.00 | 20 | 0.7 |
| 90% Sensitivity | 2.75 | 5.25 | 3.25 | 55 | 1.7 |
| Values at optimal cut-off points | | | | | |
| Sensitivity (%) | 70 | 74 | 82 | 61 | 61 |
| Specificity (%) | 66 | 65 | 49 | 73 | 78 |
| Likelihood ratio | 2.0 | 2.1 | 1.6 | 2.3 | 2.8 |

AUC, area under receiver–operator characteristics curve; CPI, C-peptide index; ΔCPR, increment of C-peptide immunoreactivity; CPR-6 min, C-peptide immunoreactivity 6 min after intravenous injection of glucagon; FCPR, fasting C-peptide immunoreactivity; SUIT, secretory unit of islet in transplantation index

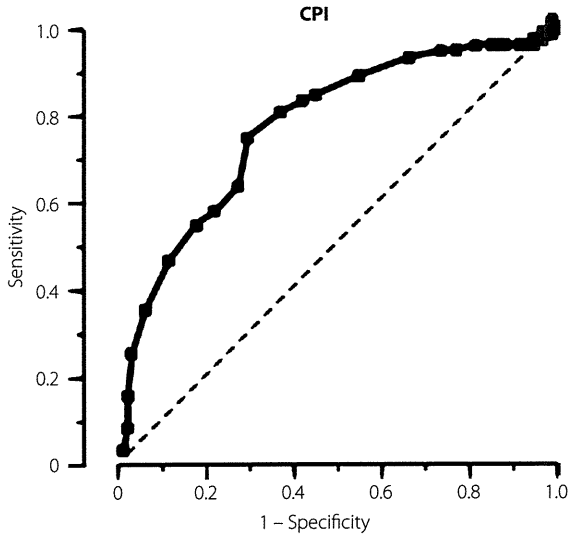


**Figure 2** | Receiver–operator characteristic curve of C-peptide index (CPI) of patients who achieved <7.4% $HbA_{1c}$ within 6 months after discharge.

In the present study, just 42% of patients achieved good control during hospital admission, partly because the aim of admission was not necessarily to achieve good control during the period of admission, but to establish a treatment policy for the achievement of good control after discharge. The percentage of patients treated with insulin at discharge was higher in the non-achieved group than in the achieved group (non-achieved group: 67%; achieved group: 41%). Of the patients treated with OHA at admission in the achieved group, 39% had therapy changed to insulin, whereas 73% of the patients treated with OHA at admission in the non-achieved group had therapy changed to insulin. These results might indicate more intensive therapy in the case of the non-achieved group. Of the 136 patients in the non-achieved group at discharge, 76 showed <7.4% $HbA_{1c}$ within 6 months after discharge, showing fair glycemic control in some of the patients of this group over the longer term. As shown in Table 1, the non-achieved group had more progressive diabetic complications and more years from diagnosis compared with the achieved group. These factors might prompt therapy that aims at a more gradual improvement of glycemic control to prevent hypoglycemia. In addition, the non-achieved group showed higher glycemic levels at admission than that of the achieved group, whereas the duration of hospitalization was similar.

Although there have been several reports regarding the utility of indices of endogenous insulin secretion to indicate initiation of insulin therapy to improve glycemic control[11–14], none has compared the utility of the various indices. In the present study, as shown by the likelihood ratio and by AUC, CPI is shown to be the most useful among the five indices.

CPI was used as an index of endogenous insulin secretion in several reports[26–28], but its advantage over other indices and the scientific basis was unclear. The SUIT index (SUIT) was developed using FCPR and plasma glucose level after islet transplantation[19]. The linear relationship between FCPR and FPG in individual subjects shows a plasma glucose level (61.7 mg/dL) assumed to suppress C-peptide to zero. Transplantation of islets from non-diabetic donors increases the slope (FCPR/[FPG − 61.7]), suggesting an index of transplanted β-cell mass. Although a correlation between SUIT and CPR 6 min after intravenous injection of 1 mg glucagon (CPR-6 min) is observed in type 2 diabetes ($r = 0.58$), it is weaker than that in patients after islet transplantation ($r = 0.82$)[19].

Autopsy reveals that β-cell mass is decreased in patients with type 2 diabetes compared with that in healthy subjects[29–31]. Recently, in 33 subjects at various stages of glucose tolerance, a correlation between β-cell areas of a sample obtained during pancreatectomy, and serum levels of CPR and insulin before the operation was analyzed[32]. Interestingly, β-cell areas are positively correlated with fasting insulin/FPG ($r = 0.51$, $P = 0.0024$) and FCPR/FPG ($r = 0.63$, $P < 0.0001$), but are not significantly

correlated with homeostasis model assessment β-cell function (HOMA-β). Because SUIT resembles HOMA-β in that insulin secretion is assumed to be suppressed to zero at approximately 60 mg/dL glucose in the formula, CPI might be a better index of residual β-cell mass than SUIT in subjects with glucose intolerance. Furthermore, CPI is not affected by exogenous insulin[27], which might favor reproducibility of the results in patients with insulin therapy. Determination of the index using a one-point blood sample without the use of loading agents also favors CPI.

In results derived from CPI of patients with mean preprandial capillary plasma glucose levels of <130 mg/dL at discharge, AUC was 0.75, optimal cut-off value was 1.1 ng/mg with 61% sensitivity and 78% specificity, and values at 90% sensitivity and at 90% specificity were 1.7 and 0.7 ng/mg, respectively. Interestingly, in results derived from CPI of patients who achieved <7.4% $HbA_{1c}$ within 6 months after discharge, AUC was 0.75, optimal cut-off value was 1.2 ng/mg with 73% sensitivity and 71% specificity, and values at 90% sensitivity and at 90% specificity were 1.7 and 0.8 ng/mg, respectively, similar to the values evaluated by mean preprandial glucose levels at discharge. These values are also similar to those in a previous report in Japanese using the data of 180 subjects from another institution (optimal cut-off value: 1.0 with 62% sensitivity and 81% specificity; values at 90% sensitivity: 1.8; 90% specificity: 0.7 ng/mg), although good glycemic control was defined as 8.4% in $HbA_{1c}$, which is somewhat inadequate[14]. Thus, CPI might be a predictor of suitable therapy to achieve fair glycemic control not only for the short-term, but also for longer duration.

The main limitation of the present study is that it is a retrospective analysis of inpatients at one hospital, and the protocol for starting insulin therapy was not defined precisely. However, in the achieved group analyzed as subjects, the decisions as to whether to start insulin therapy made by Japanese Board Certified Diabetologists were confirmed retrospectively to have been made according to the treatment guide for diabetes of the Japan Diabetes Society, as discussed in the results section.

In conclusion, we have shown the advantage of CPI of indices using CPR to select insulin therapy to achieve good glycemic control. However, limitations of the predictive abilities of indices using CPR generally and the importance of observation of the clinical therapeutic course must be taken into consideration.

## ACKNOWLEDGEMENTS

The authors declare no conflict of interest.

## REFERENCES

1. DeFronzo RA. Lilly lecture 1987. The triumvirate: β-cell, muscle, liver. A collusion responsible for NIDDM. *Diabetes* 1988; 37: 667–687.
2. Yki-Järvinen H, Kauppila M, Kujansuu E, *et al.* Comparison of insulin regimens in patients with non-insulin-dependent diabetes mellitus. *N Engl J Med* 1992; 327: 1426–1433.
3. Turner RC, Cull CA, Frighi V, *et al.* Glycemic control with diet, sulfonylurea, metformin, or insulin in patients with type 2 diabetes mellitus: progressive requirement for multiple therapies (UKPDS 49). UK Prospective Diabetes Study (UKPDS) Group. *JAMA* 1999; 281: 2005–2012.
4. Japan Diabetes Society. Diabetes mellitus: the disease itself. In: Japan Diabetes Society (ed.). *Treatment Guide for Diabetes 2007*. Bunkodo, Japan, 2007; 8–13.
5. U.K. Prospective Diabetes Study Group. U.K. prospective diabetes study 16. Overview of 6 years' therapy of type II diabetes: a progressive disease. *Diabetes* 1995; 44: 1249–1258.
6. Funakoshi S, Fujimoto S, Hamasaki A, *et al.* Analysis of factors influencing pancreatic β-cell function in Japanese patients with type 2 diabetes: association with body mass index and duration of diabetic exposure. *Diabetes Res Clin Pract* 2008; 82: 353–358.
7. Faber OK, Binder C. C-peptide response to glucagon. A test for the residual β-cell function in diabetes mellitus. *Diabetes* 1977; 26: 605–610.
8. Hendriksen C, Faber OK, Drejer J, *et al.* Prevalence of residual B-cell function in insulin-treated diabetics evaluated by the plasma C-peptide response to intravenous glucagon. *Diabetologia* 1977; 13: 615–619.
9. Jayyab AK, Heding LG, Czyzyk A, *et al.* Serum C peptide and IRI levels after administration of glucagon and glucose in non-insulin-dependent diabetics. *Horm Metab Res* 1982; 14: 112–116.
10. Gjessing HJ, Damsgaard EM, Matzen LE, *et al.* Reproducibility of β-cell function estimates in non-insulin-dependent diabetes mellitus. *Diabetes Care* 1987; 10: 558–562.
11. Madsbad S, Krarup T, McNair P, *et al.* Practical clinical value of the C-peptide response to glucagon stimulation in the choice of treatment in diabetes mellitus. *Acta Med Scand* 1981; 210: 153–156.
12. Sanke T, Satogami E, Sowa R, *et al.* Plasma C-peptide response during glucagon test as an index for evaluation of insulin requirement in diabetics (in Japanese). *J Jpn Diab Soc* 1985; 28: 713–719.
13. Koskinen P, Viikari J, Irjala K, *et al.* C-peptide determination in the choice of treatment in diabetes mellitus. *Scand J Clin Lab Invest* 1985; 45: 589–597.
14. Asano T, Kawamura M, Watanabe T, *et al.* Indices of urinary and serum C-peptide corrected with fasting plasma glucose for decision-making of insulin therapy in type 2 diabetes-validation and comparison (in Japanese). *J Jpn Diab Soc* 2008; 51: 759–763.
15. American Diabetes Association. Diagnosis and classification of diabetes mellitus. *Diabetes Care* 2010; 33: S62–S69.
16. Kajinuma H, Tanabashi S, Ishiwata K, *et al.* Urinary excretion of C-peptide in relation to renal function. In: Baba S (ed.). *Proinsulin, Insulin, C-Peptide*. Excerpta Medica, Amsterdam, 1979; 183–189.
17. American Diabetes Association. Standards of medical care in diabetes-2010. *Diabetes Care* 2010; 33: S11–S61.
18. Japan Diabetes Society (ed.). *Treatment Guide for Diabetes 2007*. Bunkodo, Japan, 2007.

 